



HAL
open science

New archeointensity data from Spain and the geomagnetic dipole moment in Western Europe over the past 2000 years

Miriam Gomez-Paccard, Annick Chauvin, Philippe Lanos, Jacques Thiriot

► **To cite this version:**

Miriam Gomez-Paccard, Annick Chauvin, Philippe Lanos, Jacques Thiriot. New archeointensity data from Spain and the geomagnetic dipole moment in Western Europe over the past 2000 years. *Journal of Geophysical Research: Solid Earth*, 2008, 113 (B9), pp.B09103. 10.1029/2008JB005582. insu-00334739

HAL Id: insu-00334739

<https://insu.hal.science/insu-00334739>

Submitted on 1 Apr 2016

HAL is a multi-disciplinary open access archive for the deposit and dissemination of scientific research documents, whether they are published or not. The documents may come from teaching and research institutions in France or abroad, or from public or private research centers.

L'archive ouverte pluridisciplinaire **HAL**, est destinée au dépôt et à la diffusion de documents scientifiques de niveau recherche, publiés ou non, émanant des établissements d'enseignement et de recherche français ou étrangers, des laboratoires publics ou privés.

New archeointensity data from Spain and the geomagnetic dipole moment in western Europe over the past 2000 years

M. Gómez-Paccard,^{1,2} A. Chauvin,¹ P. Lanos,^{1,3} and J. Thiriot⁴

Received 8 January 2008; revised 18 May 2008; accepted 16 June 2008; published 26 September 2008.

[1] Archeomagnetic studies on 14 kilns, a group of jar fragments, and a collection of baked bricks dated between 1000 and 1959 AD plus one Roman pottery kiln have been conducted in order to obtain high-quality archeointensity data to enhance the western European database. The Thellier method with corrections for anisotropy of thermoremanent magnetization (TRM) and for cooling rate dependence upon TRM acquisition was used. The effect of TRM anisotropy is only important for the bricks where the corrected and uncorrected mean intensities differ by more than 5%. Cooling rate correction factors determined per sample are up to 15% and per site up to 7.7%. Our 17 new data together with 62 previously published results were used to obtain, by Bayesian modeling, the geomagnetic field intensity over the past two millennia for western Europe. Our results indicate that geomagnetic intensity remained more or less constant between the 1st and 4th centuries and between the 14th and 16th centuries (mean values, at Paris, around 65 and 57 μT , respectively), whereas an important decrease occurs between 1600 and 1800 AD. The detailed evolution of geomagnetic field intensity during the High Middle Ages is not yet well established. Despite their differences, geomagnetic global models predict our results reasonably well. This work indicates the need to obtain a number of archeointensity data for each time interval in order to reliably record variations of the geomagnetic field and to test whether any relationship exists between field intensity and climate.

Citation: Gómez-Paccard, M., A. Chauvin, P. Lanos, and J. Thiriot (2008), New archeointensity data from Spain and the geomagnetic dipole moment in western Europe over the past 2000 years, *J. Geophys. Res.*, 113, B09103, doi:10.1029/2008JB005582.

1. Introduction

[2] The study of the evolution of the geomagnetic field requires widely distributed high-resolution magnetic records of the Earth's magnetic field. Prior to times of direct measurements [Jackson *et al.*, 2000] this can be achieved by studying the remanent magnetization of archeological material, lava flows and lake sediments. Volcanic rocks sometimes lead to low success rate or paleointensity determinations which are difficult to interpret due to the low stability of the magnetic minerals during heating. Sedimentary rocks can provide only a continuous record of the relative paleointensity changes, and the translation toward an absolute scale is not always easy. In contrast, archeomagnetic materials acquire a thermoremanent magnetization (TRM) that can be used to obtain at the

same time the paleodirection and the absolute paleointensity of the ancient Earth's magnetic field. In addition, magnetic minerals in archeomagnetic samples generally show good physicochemical stability during heating, which results in easier interpretation and high success rates (often 80% or more) of the paleointensity experiments. Thus, archeomagnetic studies of well-dated and "in situ" material can presently provide the highest-resolution description of the full-vector Earth's magnetic field over the last millennia.

[3] Archeomagnetic, volcanic and sedimentary paleomagnetic data can be used to compute spherical harmonic models of the geomagnetic field [see, e.g., Hongre *et al.*, 1998] that can offer better insight into the field evolution and underlying processes at the core mantle boundary than individual time series. A global data set of archeomagnetic and paleomagnetic data, including intensity data covering the past 7000 years, has been compiled by Korte *et al.* [2005]. This data set has been used to construct continuous global geomagnetic field models for the last millennia [Korte and Constable, 2005a]. From these spherical harmonic models, the evolution of the dipole moment during the last millennia can be obtained. It can be seen that the dipole moments predicted by Korte and Constable [2005a] are significantly lower than both those predicted by Hongre *et al.* [1998] and the virtual axial dipole moments (VADM) published by Yang *et al.* [2000]. The evolution, during the last two millennia, of the geographical coordinates of the

¹Géosciences-Rennes, UMR6118, Université de Rennes 1, CNRS, Rennes, France.

²Now at Facultat de Geologia, Departament d'Estratigrafia, Paleontologia i Geociències Marines, Universitat de Barcelona, Barcelona, Spain.

³UMR5060, IRAMAT, Maison de l'Archéologie, Université de Bordeaux 3, CNRS, Pessac, France.

⁴Laboratoire d'archéologie médiévale méditerranéenne, UMR6572, Maison méditerranéenne de Sciences de l'Homme, CNRS, Aix-en-Provence, France.

North geomagnetic pole predicted by both models is also different. These differences indicate the need to obtain more directional and intensity data in order to increase the resolution of these models. This will improve our knowledge of the evolution of the Earth's magnetic field.

[4] Archeomagnetic research started in France with the work of E. Thellier [Thellier, 1938; Thellier and Thellier, 1959] and has progressed to the stage where several directional secular variation curves for the last millennia are now available for Europe, including France [Bucur, 1994; Gallet et al., 2002], Great Britain [Batt, 1997; Zanani et al., 2007], Bulgaria [Kovacheva et al., 1998], Germany [Schnepf and Lanos, 2005], Hungary [Márton, 2003; Márton and Ferencz, 2006], Austria [Schnepf and Lanos, 2006], Spain [Gómez-Paccard et al., 2006c] and Italy [Tema et al., 2006]. However, detailed and reliable measurements of the geomagnetic intensity are now needed to fully describe the evolution of the Earth's magnetic field. Although several studies have been carried out during the last few decades in western Europe, the archeointensity data are still sparse in comparison to directional data. One compilation of the archeointensity data in western Europe for the last two millennia has been published by Chauvin et al. [2000]. This work showed that the reliability of some of the previously published data seems questionable (because they were obtained using unreliable archeointensity techniques and/or very few samples per site were considered) and provided 20 new reliable archeointensity data for France. Thus, there is a need not only to increase the quantity of data but also to improve the quality of the archeointensity determinations. Since then, new reliable results obtained from French pottery fragments have been published [Genevey and Gallet, 2002; Gallet et al., 2005]. In Spain, some archeointensity studies have been performed [Kovacheva et al., 1995; Nachasova et al., 2002, 2007; Burakov et al., 2005, 2006; Gómez-Paccard et al., 2006a], but for the last two millennia only eight archeointensity values are available.

[5] Despite such activity, the existing archeointensity data set for western Europe remains relatively poor. In order to address this deficit 15 kilns, a collection of baked bricks and a group of large jar fragments coming from seven Spanish localities have been investigated. The 17 new archeointensity data obtained have been combined with the most reliable data previously published for western Europe. The compilation of 79 data were then treated by Bayesian modeling [Lanos, 2004] to obtain the evolution of geomagnetic field intensity in western Europe for the past two millennia. Our resulting curve has been compared to one obtained using the classical moving average window method and with global geomagnetic field models. The new data enhance the European data set and will contribute to future refinement of global geomagnetic models. The intensity curve proposed should be useful for future archeomagnetic dating in this region, specially in the case of displaced objects.

2. Archeological Dating and Sampling

[6] The locations of the archeological excavations where the material was sampled are shown in Figure 1. Between 12 and 22 independently oriented samples were collected per kiln. The samples, taken from the walls, were composed of burnt clay, bricks or a mixture of them and were oriented by

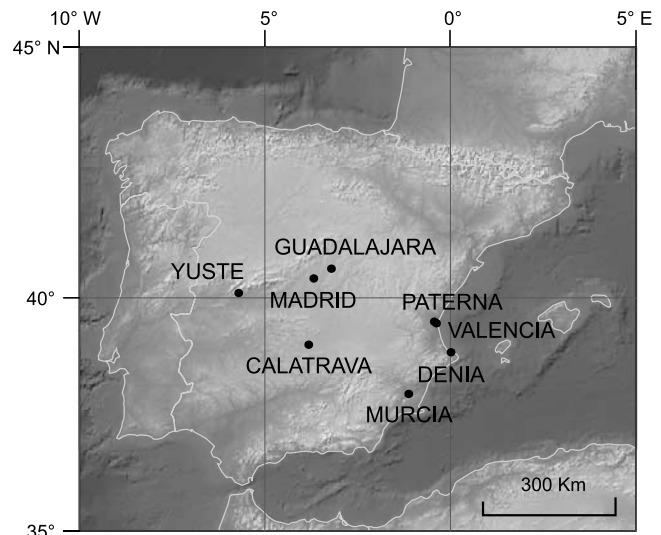


Figure 1. Map of Spain showing the location of the archeomagnetic sites where our samples were collected and Madrid.

magnetic and solar compasses on the horizontal plane of plaster coverage. Nine infill bricks (bricks GUA2 found inside the kiln GUA2) and 5 jar fragments (CERCALB baked jars fired in the kiln CALB) were also collected. In the laboratory, one standard paleomagnetic core was drilled per archeomagnetic sample. The sampling and dating methodology (mainly based on archeological constraints) are reported by Gómez-Paccard et al. [2006b]. The age of the studied samples (Table 1) ranges between the 3rd and the 20th centuries AD.

3. Archeomagnetic Directions

[7] Remanent magnetization was measured with a Molspin spinner or JR5 (AGICO) magnetometer and low field susceptibility was measured with a Bartington susceptibility meter at the paleomagnetic laboratory of Géosciences-Rennes. Our samples are characterized by a natural remanent magnetization (NRM) lower than 13 A/m and low field susceptibility between 10^{-4} and 10^{-2} SI units (Figure 2). NRM intensity and low field susceptibility are scattered both between and within sites. The original Thellier paleointensity method [Thellier and Thellier, 1959], based on the comparison between NRM lost and partial thermoremanent magnetization (pTRM) gained in a known laboratory field was used in order to determine simultaneously the characteristic directions of magnetization (for the oriented samples) and the paleointensities for all samples except for those from site GUA2. For site GUA2, the archeomagnetic direction was obtained by thermal demagnetization from oriented samples taken from the walls of the kiln where unoriented bricks studied here for paleointensity determinations were manufactured and fired. In most cases, high-quality, single components of magnetization were obtained, which likely correspond to the TRM acquired during the last firing of the structures, related to their abandonment. The experimental procedures and the archeomagnetic directions obtained (Table 1) are described by Gómez-Paccard et al. [2006b]. Figure 3 shows

Table 1. Location and Ages of the Different Group of Samples Studied and Archaeomagnetic Directions Obtained by *Gómez-Paccard et al.* [2006b]^a

	Name	Lat (°N)	Long (°E)	t_{\min}	t_{\max}	Meth.	Directional Results [<i>Gómez-Paccard et al.</i> , 2006b]					Site	Structure
							n	D_s	I_s	k	α_{95}		
1	DENA	38.86	0.02	220	250	arch	10	-4.5	52.6	669	1.9	Denia, Setla Mirarosa Miraflor	kiln
2	MURG	37.98	-1.12	1000	1100	arch	8	21.7	51.3	1437	1.5	Murcia, c/Sagasta	glass making kiln
3	CALA	39.02	-3.82	1275	1300	arch/his	8	11.4	44.9	356	2.9	Calatrava la Vieja	pottery kiln
4	CALB	39.02	-3.82	1275	1300	arch/his	10	7.1	44.4	284	2.9	Calatrava la Vieja	pottery kiln
5	CERCALB (*)	39.02	-3.82	1275	1300	arch/his						Calatrava la Vieja	jars fragments fired in CALB
6	VALN	39.47	-0.37	1238	1350	arch	9	2.1	46.6	1859	1.2	Valencia, Velluters	bricks making kiln
7	VALI	39.47	-0.37	1238	1400	arch	11	4.4	46.4	725	1.7	Valencia, Velluters	bricks making kiln
8	VALK	39.47	-0.37	1300	1450	arch	9	3.0	44.2	1606	1.3	Valencia, Velluters	glass making kiln
9	VALM	39.47	-0.37	1300	1450	arch	9	7.2	47.0	2733	1.0	Valencia, Velluters	glass making kiln
10	CALC	39.02	-3.82	1400	1420	arch/his	8	3.0	47.0	790	2.0	Calatrava la Vieja	pottery kiln
11	PATA	39.50	-0.43	1450	1500	arch	10	3.6	56.4	792	1.7	Paterna, c/Huertos	pottery kiln
12	PATJ	39.50	-0.43	1429	1611	C14	16	6.6	62.2	1201	1.1	Paterna, Testar del Moli	pottery kiln
13	PATH	39.50	-0.43	1450	1600	arch	10	7.3	53.5	831	1.7	Paterna, Testar del Moli	pottery kiln
14	PATB	39.50	-0.43	1525	1650	arch	11	5.8	64.1	827	1.6	Paterna, c/Huertos	pottery kiln
15	VALL	39.47	-0.37	1575	1625	arch	11	9.1	56.6	557	1.9	Valencia, Velluters	Kiln
Not studied here	GUA2	40.60	-3.20	1825	1845	arch/his	13	-21.1	61.5	238	2.7	Guadalajara, Huertas del Carmen	Furnace
16	BRICKS GUA2 (*)	40.60	-3.20	1825	1845	arch/his							Brick fragments fired in GUA2
17	YUS2	40.10	-5.70	1959	1959	his	5	-11.1	58.2	138	6.5	Yuste, monastery	Kiln

^aColumns from left to right: No, number; Name, name; Lat. and Long., latitude and longitude of the sampling site; t_{\min} , minimum age in years AD; t_{\max} , maximum age in years AD; Meth., method of dating (arch.: archaeological age estimate, hist: historical document, C14: calibrated ¹⁴C); n , number of samples taken into account in the calculation of the mean site direction; D_s and I_s , declination and inclination in situ; k and α_{95} , precision parameter and 95% confidence limit of characteristic remanent magnetization; Site; site name; Structure, kind of structure. (*) number 5 are jar fragments fired in the kiln CALB and number 16 are brick fragments fired in the kiln GUA2.

the results relocated to Paris together with the secular variation curve for France [*Gallet et al.*, 2002] implemented using Bayesian statistics [*Lanos*, 2004]. The directions of magnetization were relocated to Paris via the virtual geomagnetic pole (VGP). It can be seen that mean directions of magnetization for structures of the same age are very similar, with their circles of confidence (α_{95}) overlapping (as for example for CALA-B, or VALN-I). The structures PATB and PATJ, with large age uncertainties, seem to be contemporaneous. Despite some differences, the archeomagnetic directions obtained show the same general pattern as the French secular variation curve, indicating consistency with the proposed archeological dates [*Gómez-Paccard et al.*, 2006c].

4. Magnetic Mineralogy

[8] Low field susceptibility versus temperature curves (K - T curves), isothermal remanent magnetization (IRM) acquisition and thermal demagnetization of composite IRM have been carried out in order to determine the principal magnetic carrier in our samples. Thermomagnetic curves were performed in air using a KLY3 (Agico) susceptibility meter with fitted furnace. IRM was obtained using an ASC Scientific impulse magnetizer. One sample has been also analyzed by scanning electron microscopy (SEM) and energy dispersive X-ray analysis.

4.1. K - T Curves

[9] A total of 109 K - T experiments up to 700°C were performed. Heating and cooling curves are reasonably reversible, suggesting that few mineralogical changes occurred during heating (Figure 4). Curie temperatures (T_c) between

350°C and 650°C were observed. In some cases only one magnetic phase is present (Figures 4a and 4c) and in others two clear magnetic phases, one of low T_c (around 350–400°C) and another of high T_c (Figure 4b). Generally, the T_c of this high- T_c component ranges between 550 and 585°C. Some samples have a T_c higher than 585°C, which can be interpreted in terms of partially oxidized (titano)magnetite or (titano)maghemite or hematite (Figure 4d). Thermomagnetic curves suggest that the principal magnetic phase present in our samples is magnetite or titanomagnetite with different Ti content. Some stable Al, Na, Mg substituted maghemite (with low T_c) could also be present. Curie temperatures are in agreement

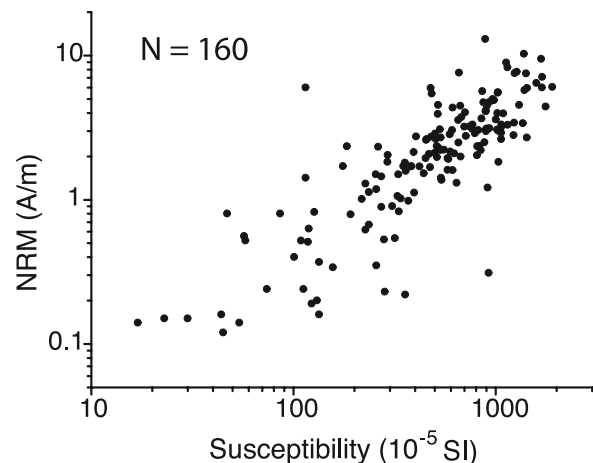


Figure 2. Natural remanent magnetization (NRM) intensity (A/m) versus susceptibility (10^{-5} SI units) for all samples.

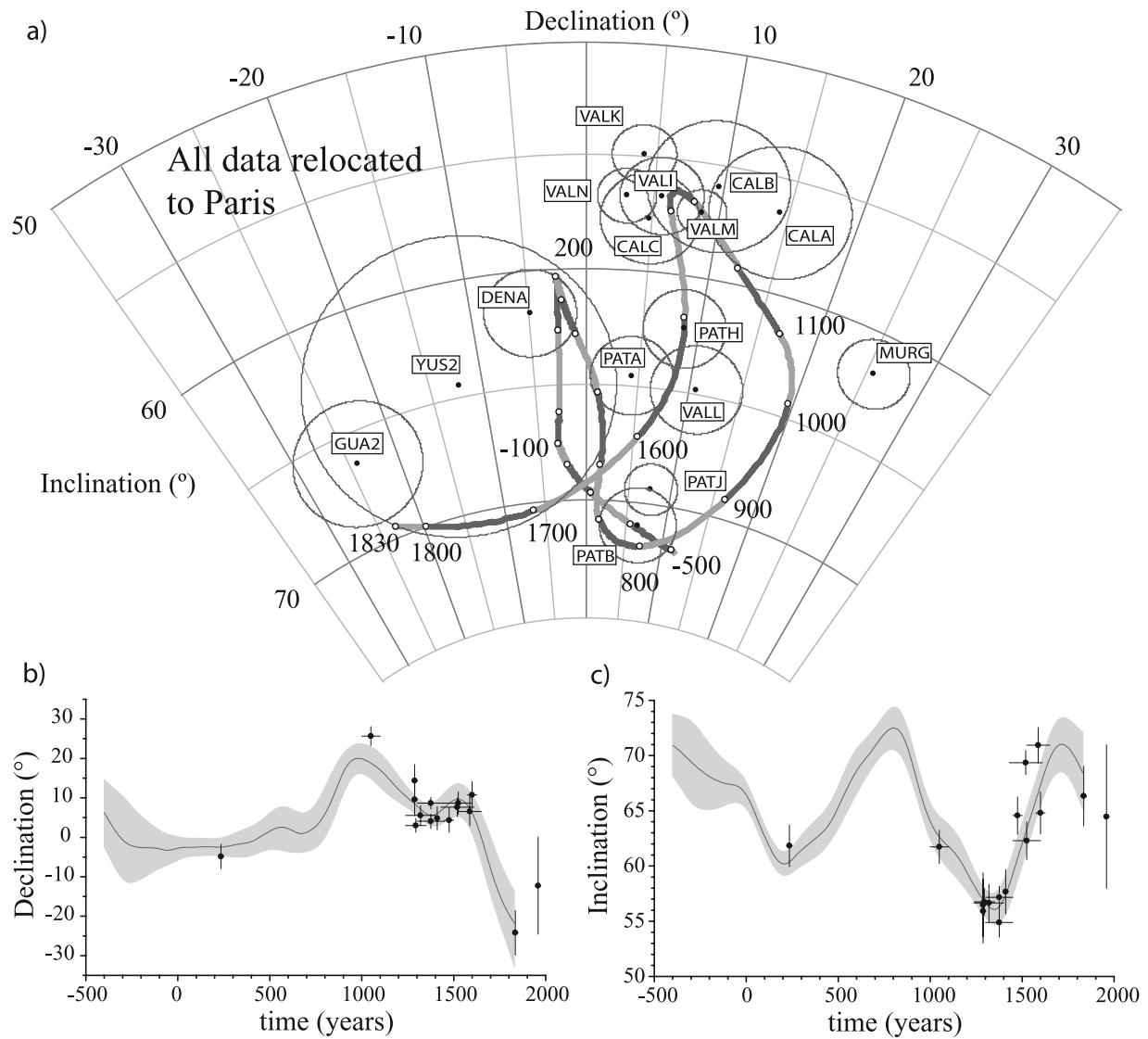


Figure 3. (a) Stereographic projection of mean directions of magnetization with α_{95} error circles [Fisher, 1953] of the studied Spanish structures, (b and c) declination and inclination of mean direction. The French secular variation curve, obtained by Bayesian modeling, is also plotted. All data are relocated to Paris (latitude 48.9° N, longitude 2.3° E).

with the unblocking temperatures observed during the Thellier experiments.

4.2. IRM Acquisition and Thermal Demagnetization of Composite IRM

[10] Fifty-five samples (from all studied sites) were analyzed by progressive acquisition of IRM. In most cases saturation is reached for fields between 50 and 150 mT (Figure 5a). This suggests that magnetization is carried by low-coercivity magnetic minerals such as titanomagnetite or magnetite. A gradual increase in the intensity of the IRM up to the maximum magnetizing field of 1150 mT is observed in some samples (Figures 5b and 5c), suggesting the presence of hematite or titanohematite.

[11] Thermal demagnetization of three-axes composite IRM [Lowrie, 1990] was also conducted on the same set of samples. IRM acquisitions were performed in three steps.

First, the samples were remagnetized in a field of 1150 mT along their z axis, then a second IRM was given along their x axis in a field of 300 mT, and finally a third IRM was given along their y axis in a field of 150 mT. The thermal demagnetization of each orthogonal component is then analyzed separately (Figure 5). Usually the low-coercivity IRM along the y axis has the highest intensity and its unblocking temperatures ranges between 350°C and 600°C (Figures 5a and 5b). In a few samples from three sites (VALI, GUA2 and YUS2) the magnetization acquired along the z axis (in 1150 mT) has unblocking temperatures above 650°C (Figures 5b and 5c). This suggests the presence of hematite. Goethite was also recognized in some samples (Figure 5b). These experiments again suggest that the main magnetic carrier in our samples is magnetite or titanomagnetite with different Ti contents.

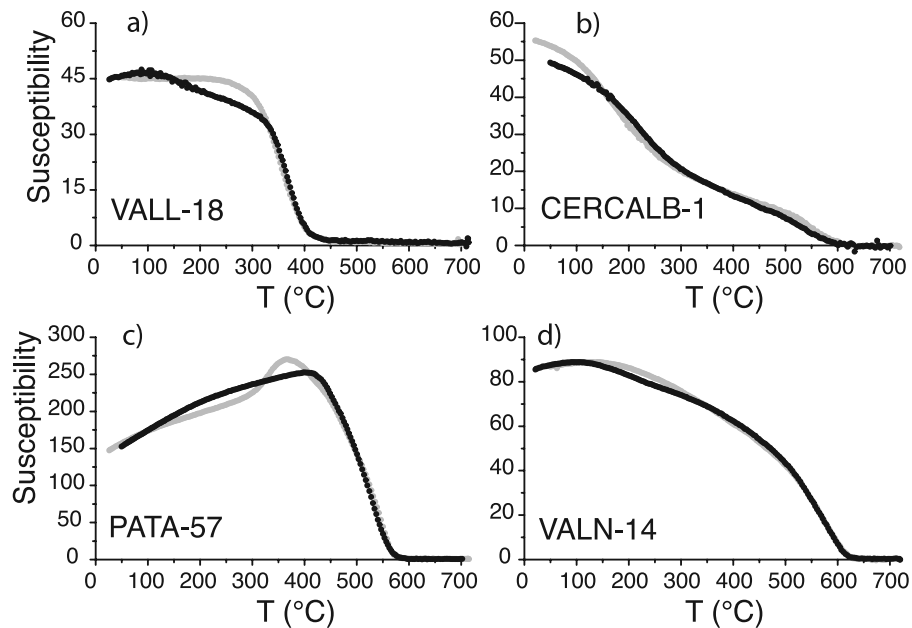


Figure 4. Examples of typical susceptibility versus temperature curves (K - T curves). Susceptibilities are in arbitrary units. Heating (cooling) branches are plotted in black (gray) circles.

4.3. SEM and Energy Dispersive X-Ray Analysis

[12] SEM and energy dispersive X-ray analysis were carried out on sample VALI-13 where hematite was detected (see Figure 5b). For this purpose we used a conventional SEM JSM-6400 and an energy-dispersion spectrometer OXFORD Link Isis in the C.M.E.B.A. at the University of Rennes 1. SEM experiments confirm the previous results: titanomagnetite and hematite were found in this sample. The particle shown in Figure 6a (titanomagnetite: for this particle the X-ray analysis confirm the presence of O, Fe and Ti but the numerical results are biased by the presence of C contained in the matrix of the bulk sample) is supposed to represent the low-coercivity (less than 150 mT) magnetic phase observed in VALI-13. The particle shown in Figure 6b (hematite: 47.16% of O and 31.62% of Fe) corresponds to the magnetic phase which does not reach saturation at 1150 mT (see IRM results).

5. Archeointensity Determinations

5.1. Experimental Procedure

[13] The original Thellier method [Thellier and Thellier, 1959] with pTRM checks was used. The TRM anisotropy tensor and cooling rate dependence of TRM intensity were determined for each sample. The paleointensity results were then corrected for these effects. For a detailed description of experimental procedures and selection criteria used see Gómez-Paccard *et al.* [2006a]. A laboratory field of 50 or 60 μT was applied during heating and cooling along the cylindrical axis (z) of the samples. Samples were heated in air in a Magnetic Measurements oven, from 100°C until more than the 85% of the initial NRM was lost, using between 7 and 19 temperature steps.

[14] The archeological information available for the studied structures suggests that the cooling time in the archeological site was probably 1 or 2 days. Thus, two cooling

times of 24 and 48 h have been used in order to quantify the cooling rate effect upon TRM intensity in our samples. The correction factors per sample and the corresponding alteration (that occurred during the heatings carried out in order to estimate the cooling rate correction factor) have been calculated.

5.2. NRM-TRM Diagrams

[15] Paleointensity determinations were attempted on 175 samples, and 160 of them have given reliable results. The very high success rate of more than 90% shows the excellent physical and chemical stability of the magnetic minerals contained in our samples. The acceptance criteria used here are the same as those described by Gómez-Paccard *et al.* [2006a]. All accepted results at sample level are given in Table 2. The high-quality NRM-TRM diagrams observed (see Figure 7) allow us to obtain archeointensity determinations from fractions of the NRM component (f factor) bigger than 0.5, maximum angle of deviation (MAD) lower than 5.5° and deviation angle (DANG) lower than 5°. Only for four samples the potential error on the estimation of the paleointensity due to the acquisition of chemical remanent magnetization (CRM) as a percentage of the applied field obtained is bigger than 10% (Figure 8 and Table 2). In order to calculate the mean site intensities the weighting factor per specimen proposed by Prévot *et al.* [1985] has been used. The dispersion around the mean is expressed as the standard deviation (s.d.). For the unoriented bricks and jar fragments the archeomagnetic direction of the corresponding structure (Table 1) has been used in order to calculate the virtual dipole moment (VDM).

5.3. TRM Anisotropy

[16] TRM anisotropy has been determined for 157 samples. For the majority of the samples the degree of TRM anisotropy k_1/k_3 (where k_1 and k_3 are the maximum and minimum axes

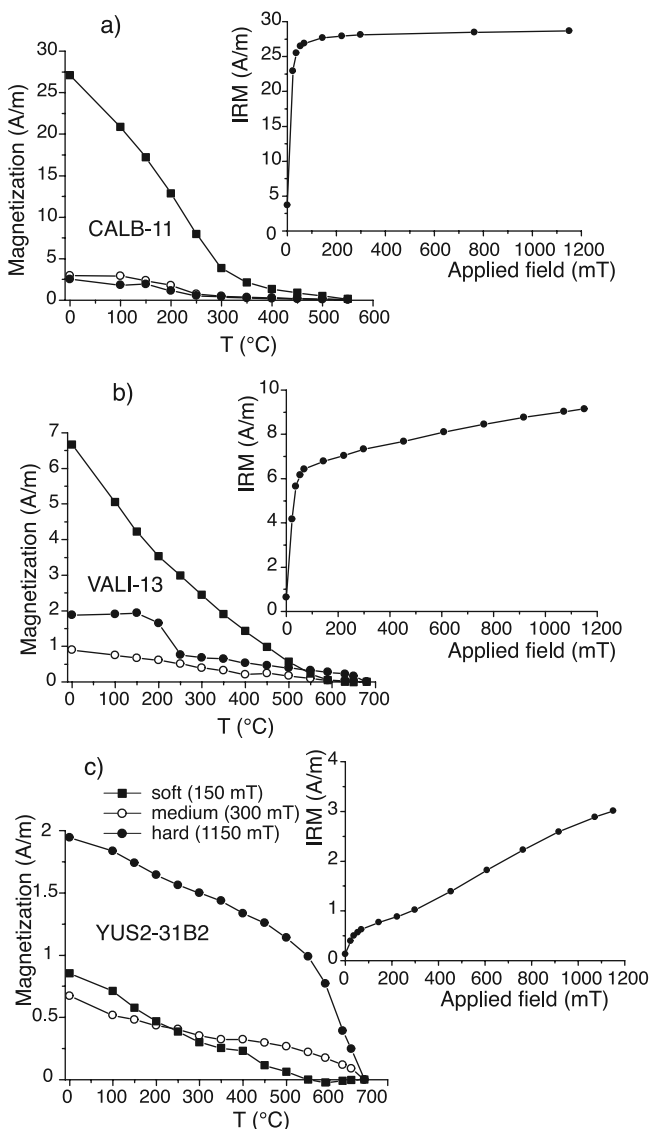


Figure 5. Representative examples of isothermal remanent magnetization (IRM) acquisition curves and thermal demagnetization of three-axis IRM.

of the tensor of TRM anisotropy) were generally lower than 10%. There is no dominance of magnetic lineation or foliation and the directions of the principal axes of the tensors are scattered within almost all the sites. Figure 9a shows an example (CALA) of this general behavior.

[17] The infill bricks (bricks GUA2) are the exception. In this case higher degrees of TRM anisotropy, were found and magnetic foliation dominates (Figure 9b). All the samples from GUA2 were drilled perpendicular to the flattening plane of the bricks. The easy plane of magnetization is contained in the flattening plane (XY plane of the sample) of the bricks and the hard direction of magnetization is along the z axis of the samples.

[18] The random directions of the principal axes of the tensors, together with the generally low degrees of TRM anisotropy, explain the similarity of the mean intensities and mean directions of magnetization per site before and after correction (Table 3). Only for bricks GUA2 the differences

between the mean site intensity before and after TRM anisotropy correction are significant (5.7%).

5.4. Dependence of Cooling Rate Upon TRM Intensity

[19] The correction factors and the corresponding alterations obtained for a linear cooling of 24 h are shown in Figure 10a. Figure 10b shows the correction factors retained per sample and applied to the archeointensity determinations, plotted in Figure 10a in the “accepted” zone. When the correction factors were lower than the alteration factors, no cooling rate correction was applied (“rejected” zone in Figure 10a). In these cases it is not possible to estimate if the TRM acquisition capacity has changed because of the cooling rate effect or because of mineralogical changes. The uncorrected intensity values were retained in order to calculate the mean intensity per site.

[20] The correction per sample upon the archeointensity is typically lower than 10%, but can reach values up to 14% (Figure 10b). A big variability between samples of the same archaeological site is observed (see Figure 10a), suggesting that the cooling rate effect is highly dependent of the particular magnetic mineralogy of the samples. This indicates the necessity of carrying out the correction for each sample. Alteration is typically lower than 5% (Figure 10a).

[21] The mean site correction factors (overestimation of the paleointensity) are important (bigger than 5%) for four sites, moderate (between 3 and 5%) for five, and not so significant (less than 3%) for the other 8 sites. The maximum value of overestimation (7.7%) was found for the kiln VALI. For one of the kilns, MURG, the mean site correction factor is +0.5% (the paleointensity mean is an underestimate). The decrease of TRM intensity as the cooling rate decreases has been associated in the literature

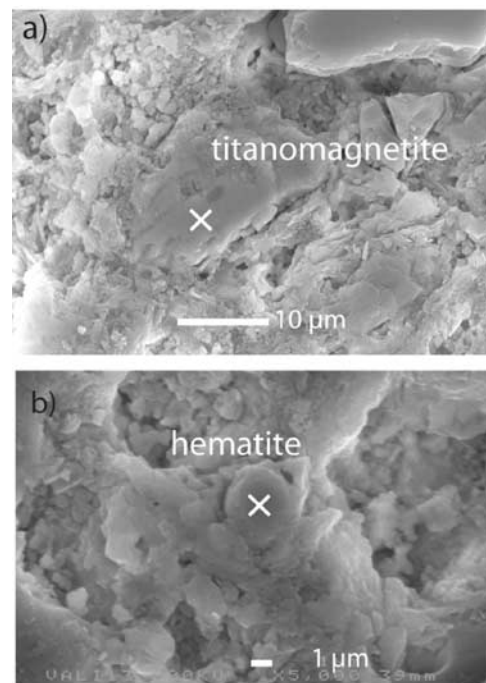


Figure 6. Examples of scanning electron microscopy observations. Points where energy dispersive X-ray analyses were done are marked by white crosses (see section 4.3).

Table 2. Archeointensity Results per Sample^a

Name (Age)	Sample Number	NRM (A/m)	χ (10^{-5})	Q	$T_{\min}-T_{\max}$ (°C)	n	f	g	q	MAD (°)	DANG (°)	CRM (%)	$F \pm \sigma F$ (μT)	F_c (μT)	
DENA 220–250	82-A	3.20	700	11.50	100–560	14	0.77	0.91	56.1	1.6	0.7	4.6	58.4 ± 0.8	58.5	
	83-A	1.80	356	12.71	100–530	13	0.64	0.90	24.6	2.5	1.7	3.7	60.3 ± 1.5	64.0	
	84-A	1.97	513	9.65	100–500	12	0.68	0.91	29.5	1.9	0.3	2.4	61.2 ± 1.3	61.1	
	85-A	5.56	1029	13.59	100–560	13	0.86	0.89	48.0	2.3	1.0	3.3	58.1 ± 1.0	55.8	
	86-A	5.43	483	28.25	100–530	13	0.84	0.89	41.3	1.7	1.8	5.7	53.9 ± 1.0	53.4	
	88-A	5.94	478	31.20	100–450	10	0.68	0.87	20.0	4.9	2.5	12.2	62.1 ± 2.0	58.0	
	89-A	2.29	522	11.04	100–560	14	0.86	0.92	48.3	1.7	1.1	5.5	62.1 ± 1.0	61.3	
	90-A	1.21	913	3.32	100–530	13	0.78	0.91	45.9	2.4	0.8	2.4	58.1 ± 0.9	60.8	
	91-A	1.99	671	7.45	100–530	13	0.73	0.91	37.9	2.3	0.5	3.7	56.9 ± 1.0	57.4	
	92-A	2.70	536	12.64	100–560	14	0.87	0.92	68.3	1.6	0.7	3.6	59.5 ± 0.7	59.7	
	MURG 1000–1100	1-B	0.31	926	0.8	150–320	5	0.51	0.73	4.0	3.3	0.4	4.2	47.2 ± 4.5	48.7
		2-B	0.52	58	22.5	100–480	11	0.90	0.89	47.5	1.1	0.4	1.1	74.4 ± 1.3	74.0
3-B		8.25	1145	18.1	100–390	8	0.90	0.83	49.8	1.9	0.9	3.2	56.3 ± 0.8	55.0	
10-A		0.16	134	3.0	100–360	7	0.79	0.79	31.4	2.2	0.5	2.0	55.4 ± 1.1	54.4	
11-A		0.34	157	5.4	100–420	9	0.78	0.84	66.7	1.8	0.2	2.2	58.6 ± 0.5	56.2	
12-A		0.4	101	10.0	100–450	10	0.79	0.79	31.4	2.2	0.5	2.0	55.8 ± 1.7	55.0	
13-A		5.99	115	130.9	100–480	11	0.78	0.89	45.3	1.9	0.5	3.6	63.4 ± 1.0	60.4	
17-A		0.01	10	2.5	280–420	5	0.41	0.74	9.3	1.7	2.5	3.9	41.9 ± 1.4	40.5	
CALA 1275–1300		2-A	5.65	859	16.5	100–530	12	0.83	0.90	38.2	2.6	0.6	3.1	58.7 ± 1.1	57.7
		4-A	3.07	530	14.6	100–560	13	0.88	0.90	160.0	1.6	0.5	1.4	57.0 ± 0.3	57.6
	6-A	2.15	597	9.1	100–560	13	0.88	0.91	56.1	2.3	0.4	4.1	60.0 ± 0.8	62.8	
	7-A	2.49	655	9.6	100–560	13	0.84	0.91	116.1	1.6	0.3	1.7	55.8 ± 0.4	58.3	
	8-A	3.03	610	12.5	100–500	11	0.88	0.89	54.7	1.4	0.4	2.0	61.4 ± 0.8	61.7	
	10-A	2.32	263	22.2	100–500	11	0.91	0.89	113.6	1.1	0.4	1.8	57.7 ± 0.4	58.7	
	11-A	1.52	441	8.7	100–560	13	0.85	0.91	45.2	2.5	0.9	3.0	57.8 ± 1.0	60.4	
	13-A	7.54	1241	15.3	100–530	12	0.85	0.90	40.6	1.9	0.5	2.2	55.8 ± 1.0	57.0	
CALB 1275–1300	14-A	2.11	500	10.6	100–360	7	0.50	0.83	26.8	1.6	3.4	1.8	65.7 ± 1.0	65.3	
	1-B	1.60	614	6.6	100–530	14	0.83	0.91	30.9	2.7	1	4.5	56.2 ± 1.4	57.1	
	2-B	4.89	983	12.5	100–410	10	0.75	0.86	28.7	2.8	0.2	3.2	63.9 ± 1.4	64.7	
	3-A	4.73	871	13.7	100–500	13	0.85	0.91	61.4	2.0	0.5	1.9	63.1 ± 0.8	61.0	
	4-A	2.22	555	10.1	100–500	13	0.80	0.92	45.3	3.1	1.9	2.9	55.7 ± 0.9	55.6	
	6-A	1.70	383	11.2	100–530	14	0.85	0.92	17.4	3.9	0.8	8.8	56.2 ± 2.5	55.0	
	7-B	1.18	257	11.5	100–530	14	0.87	0.92	61.8	4.1	0.5	4.1	53.5 ± 0.7	53.6	
	8-B	1.50	330	11.4	100–500	13	0.87	0.92	47.8	5.0	0.5	2.7	51.9 ± 0.8	50.4	
	9-A	3.09	766	10.1	100–560	15	0.86	0.91	69.5	3.4	1.6	3.4	58.7 ± 0.7	54.9	
	13-A	1.29	227	14.3	100–560	15	0.82	0.81	33.8	3.6	3.4	2.4	61.1 ± 1.3	60.4	
	14-B	1.61	579	7.0	100–560	15	0.83	0.92	36.9	3.2	0.4	3.5	53.4 ± 1.1	53.7	
	CERCALB 1275–1300	1-A	0.35	257	3.4	150–470	9	0.48	0.85	5.8	3.6	1.1	7.0	46.0 ± 3.2	46.3
		2-A	2.74	404	17.0	100–530	12	0.85	0.90	34.9	1.8	0.9	2.1	49.2 ± 1.1	52.4
		4-A	1.83	292	15.8	200–440	7	0.54	0.83	9.9	4.7	1.7	3.1	51.3 ± 2.3	56.6
6-A		0.63	119	13.3	320–600	10	0.58	0.88	22.9	2.7	2.4	5.7	71.1 ± 1.6	62.9	
VALN 1238–1350	1-A	3.96	1090	9.14	100–540	13	0.77	0.91	102.1	2.7	0.4	2.7	53.1 ± 0.4	52.7	
	2-A	2.09	624	8.40	100–540	13	0.81	0.91	43.1	2.1	0.7	3.6	50.2 ± 0.9	49.9	
	4-A	1.71	383	11.21	100–540	13	0.83	0.91	57.2	2.0	0.9	2.1	46.2 ± 0.6	44.5	
	5-A	1.70	420	10.17	100–540	13	0.82	0.91	69.1	2.7	1.0	3.2	48.9 ± 0.6	45.6	
	6-A	2.21	536	10.36	100–540	13	0.83	0.91	68.4	1.7	0.9	2.2	49.1 ± 0.6	49.0	
	7-A	2.07	469	11.09	100–540	13	0.80	0.92	57.5	2.6	1.7	3.1	50.5 ± 0.7	50.7	
	9-A	3.12	934	8.40	100–540	13	0.78	0.90	76.7	3.5	1.5	4.6	52.6 ± 0.5	52.6	
	12-A	2.89	791	9.19	100–540	13	0.85	0.91	82.4	1.8	1.2	3.7	50.3 ± 0.5	50.9	
	14-A	3.60	1004	9.02	100–540	13	0.79	0.91	102.9	3.1	2.2	4.5	55.8 ± 0.4	54.6	
	16-A	2.80	1228	5.72	100–540	13	0.73	0.91	36.9	4.3	3.2	7.8	51.9 ± 1.0	52.2	
VALI 1238–1400	18-A	2.63	1066	6.19	100–540	13	0.79	0.92	52.2	3.2	3.3	6.1	53.1 ± 0.8	51.9	
	5-A	2.03	810	6.3	100–450	10	0.65	0.89	20.9	2.8	0.7	3.5	54.5 ± 1.5	52.2	
	6-A	1.12	396	7.1	100–540	13	0.72	0.91	22.8	2.5	1.5	4.6	57.0 ± 1.6	57.8	
	8-A	3.01	1031	7.4	100–540	13	0.77	0.91	32.2	1.6	1.9	1.7	57.5 ± 1.3	57.1	
	11-A	1.37	540	6.4	100–540	13	0.80	0.91	71.4	2.1	0.8	2.3	52.9 ± 0.6	54.2	
	12-A	1.01	218	11.6	100–540	13	0.76	0.91	40.7	2.3	1.0	3.1	55.9 ± 1.0	56.4	
	13-A	1.58	360	11.0	100–480	11	0.67	0.90	29.8	2.2	2.3	4.5	57.2 ± 1.2	58.3	
	14-B	2.98	898	8.3	100–510	12	0.73	0.90	24.1	5.3	4.7	7.2	58.2 ± 1.7	58.4	
	17-B	0.89	272	8.2	100–510	12	0.77	0.91	52.1	2.8	0.8	1.9	48.1 ± 0.7	49.2	
	18-A	2.20	845	6.5	100–510	12	0.78	0.91	35.1	2.3	0.9	3.2	51.7 ± 1.1	53.0	
	19-A	0.62	227	6.9	100–510	12	0.64	0.91	27.2	3.2	1.5	4.4	50.6 ± 1.1	51.8	
	21-A	0.90	308	7.3	100–510	12	0.62	0.90	31.6	2.9	3	7.1	55.0 ± 1.0	56.9	
	VALK 1300–1450	1-A	1.94	579	8.4	100–450	10	0.52	0.87	19.9	3.5	0.8	4.0	57.6 ± 1.2	54.0
		2-A	8.91	1128	19.9	100–560	15	0.88	0.90	65.4	0.6	0.0	1.5	57.3 ± 0.7	55.9
4-A		0.67	236	7.1	100–560	15	0.87	0.90	53.6	0.8	0.0	2.4	60.7 ± 0.8	56.4	
5-A		0.37	134	6.9	100–560	15	0.85	0.92	64.0	1.3	0.0	3.4	60.5 ± 0.7	56.4	
11-A		5.95	1433	10.4	100–580	16	0.89	0.92	83.6	0.8	0.0	2.5	57.2 ± 0.5	56.0	
12-A		0.24	74	8.2	200–560	13	0.77	0.91	59.9	1.6	0.5	2.5	61.2 ± 0.7	59.8	
13-A		2.34	811	7.3	100–560	13	0.75	0.91	60.3	2.1	1.2	2.5	58.2 ± 0.7	57.2	
14-B		7.51	1417	13.3	100–560	15	0.87	0.92	55.8	1.8	0.9	2.1	52.3 ± 0.7	49.6	
15-B		2.64	505	13.1	100–500	12	0.69	0.90	34.8	2.5	1.9	2.9	51.8 ± 0.9	48.6	

Table 2. (continued)

Name (Age)	Sample Number	NRM (A/m)	χ (10^{-5})	Q	T_{\min} - T_{\max} ($^{\circ}$ C)	n	f	g	q	MAD ($^{\circ}$)	DANG ($^{\circ}$)	CRM (%)	$F \pm \sigma F$ (μ T)	F_c (μ T)	
VALM 1300–1450	1-A	0.53	281	4.7	100–450	10	0.71	0.88	12.5	4.0	1.2	6.3	58.2 \pm 2.9	58.6	
	2-A	1.42	537	6.6	100–420	9	0.82	0.84	33.3	1.9	1.2	3.4	46.8 \pm 1.0	46.8	
	3-A	6.45	1590	10.2	100–560	15	0.76	0.92	32.8	2.5	0.4	2.5	46.2 \pm 1.0	47.4	
	4-A	3.07	897	8.6	100–560	15	0.80	0.92	56.4	1.6	0.5	3.1	53.8 \pm 0.7	53.9	
	6-A	1.31	642	5.1	100–560	15	0.84	0.92	65.1	1.5	0.9	2.4	54.8 \pm 0.7	52.7	
	7-A	3.41	1235	6.9	100–560	15	0.86	0.93	66.3	1.9	0.9	2.5	50.4 \pm 0.6	48.6	
	8-A	5.99	1695	8.9	100–560	15	0.82	0.93	54.0	2.1	0.6	2.3	49.8 \pm 0.7	49.0	
	12-A	2.91	1065	6.9	100–480	11	0.68	0.89	26.8	2.6	2.0	3.5	48.6 \pm 1.1	47.3	
	14-A	3.18	1067	7.5	100–480	11	0.68	0.89	21.0	2.5	3.0	4.6	47.5 \pm 1.4	44.9	
	CALC 1400–1420	1-A	1.71	176	24.4	100–530	12	0.88	0.90	62.4	2.6	0.4	1.3	50.5 \pm 0.7	50.1
		2-A	0.51	118	10.9	100–530	12	0.74	0.86	50.1	3.0	1.8	3.8	53.9 \pm 0.7	49.0
		4-A	0.98	371	6.6	100–500	11	0.82	0.89	73.9	1.9	0.9	2.3	56.0 \pm 0.5	54.2
		8-A	0.83	332	6.3	100–500	11	0.83	0.89	57.3	1.7	1.2	2.3	54.9 \pm 0.7	53.0
		9-A	0.20	131	3.8	100–440	9	0.76	0.84	62.1	1.9	0.1	1.7	52.1 \pm 0.5	51.8
10-A		1.06	327	8.1	100–500	11	0.82	0.90	45.8	1.8	0.2	1.1	48.5 \pm 0.8	47.7	
11-A		0.82	127	16.2	100–440	9	0.66	0.87	72.6	2.0	3.8	3.6	48.5 \pm 0.4	47.2	
16-A		0.56	57	24.7	100–500	11	0.83	0.89	75.4	1.8	0.8	1.7	52.7 \pm 0.5	51.3	
17-A		1.42	115	31.0	100–500	11	0.86	0.89	110.2	1.8	0.7	2.2	47.8 \pm 0.4	48.0	
PATH 1450–1600		1-A	2.35	831	7.1	100–400	9	0.81	0.86	22.9	4.6	0.4	11.3	54.1 \pm 1.6	54.4
	3-B	0.54	318	4.3	100–400	9	0.52	0.83	12.5	3.4	1.0	8.3	64.3 \pm 2.3	64.3	
	4-A	0.22	357	1.5	100–325	6	0.69	0.78	11.5	4.3	2.4	11.3	59.7 \pm 2.9	62.0	
	5-B	0.24	112	5.4	100–550	15	0.81	0.92	40.3	2.6	1.3	4.6	54.7 \pm 1.0	54.7	
	6-A	1.02	339	7.6	100–550	15	0.83	0.92	53.6	2.9	1.1	2.8	51.8 \pm 0.8	51.6	
	7-A	3.11	906	8.6	100–400	9	0.84	0.85	30.4	2.8	0.8	3.1	53.7 \pm 1.3	54.2	
	8-A	0.16	44	9.1	100–600	17	0.88	0.93	59.5	2.5	3.2	5.1	57.1 \pm 0.8	55.3	
	10-A	4.13	895	11.6	100–450	10	0.88	0.87	36.5	1.2	1.5	1.8	51.3 \pm 1.1	51.2	
	11-A	0.14	54	6.5	100–475	12	0.67	0.90	19.0	4.9	2.3	4.3	53.8 \pm 1.7	55.1	
	12-A	0.12	45	6.7	100–600	17	0.92	0.93	50.3	2.0	0.6	2.5	48.9 \pm 0.9	52.3	
	PATA 1450–1500	50-A	9.48	1683	14.2	100–525	15	0.89	0.92	64.4	2.0	0.5	4.2	55.4 \pm 0.7	55.1
		51-A	10.25	1381	18.7	100–550	17	0.68	0.92	54.8	2.9	0.8	3.8	48.4 \pm 0.6	45.5
52-A		5.75	1390	10.4	100–450	13	0.75	0.86	30.3	2.2	1.0	5.0	52.4 \pm 1.1	53.6	
53-A		3.39	1366	6.2	100–425	12	0.66	0.88	28.0	3.7	2.0	6.9	50.0 \pm 1.1	50.8	
54-A		4.42	1770	6.3	100–425	12	0.63	0.88	17.3	4.2	1.7	9.7	48.2 \pm 1.5	45.2	
55-A		6.05	1905	8.0	100–575	18	0.88	0.86	57.9	3.8	3.1	7.9	47.2 \pm 0.6	45.2	
56-A		3.30	1150	7.2	100–450	11	0.83	0.81	38.6	2.4	0.4	4.2	55.5 \pm 1.0	56.3	
57-B		7.09	1702	10.5	100–350	9	0.77	0.79	45.5	1.9	0.9	5.3	56.3 \pm 0.8	57.7	
58-A		5.51	1025	13.5	100–600	19	0.92	0.92	105.6	2.2	0.8	4.3	56.2 \pm 0.5	56.4	
62-A		3.31	769	10.8	100–525	16	0.70	0.90	39.3	3.4	1.2	4.8	50.8 \pm 0.8	51.8	
PATB 1525–1650		1-A	2.14	394	13.62	100–500	12	0.67	0.88	23.8	2.0	1.4	7.2	48.8 \pm 1.2	47.9
	2-A	1.94	451	10.82	100–590	15	0.87	0.91	60.5	2.2	1.5	3.7	47.3 \pm 0.7	47.6	
	3-A	4.54	1308	8.71	100–390	8	0.52	0.85	10.4	2.1	3.2	8.4	60.4 \pm 2.6	59.0	
	4-A	4.74	932	12.78	100–480	11	0.83	0.88	33.0	1.3	0.8	6.3	50.6 \pm 1.2	49.9	
	5-B	2.35	512	11.54	100–530	13	0.86	0.91	31.8	4.3	1.2	11.5	48.3 \pm 1.2	46.5	
	6-A	1.83	1035	4.45	100–330	6	0.52	0.80	6.3	4.0	1.4	8.5	52.8 \pm 3.5	52.3	
	7-A	4.53	520	21.89	150–390	7	0.78	0.78	41.8	1.1	1.2	3.4	49.2 \pm 0.7	49.2	
	8-A	4.09	894	11.50	100–330	6	0.69	0.75	15.1	1.2	1.4	3.0	58.6 \pm 2.0	58.4	
	11-A	4.97	968	12.89	100–390	8	0.55	0.85	9.6	2.1	3.2	5.7	54.3 \pm 2.7	51.6	
	12-A	2.76	713	9.72	100–480	11	0.78	0.89	23.9	2.8	1.5	5.6	53.2 \pm 1.6	51.9	
	14-A	4.45	904	12.36	100–480	11	0.84	0.90	34.4	3.0	1.0	6.1	50.0 \pm 1.2	48.3	
	20-A	3.06	1019	3.06	100–330	6	0.74	0.79	12.0	2.9	1.3	8.0	58.1 \pm 2.8	60.1	
	PATJ 1429–1611	40-A	3.57	654	13.72	100–525	14	0.82	0.90	48.3	2.1	1.9	6.9	51.2 \pm 0.8	52.8
41-A		1.50	256	14.74	100–575	16	0.88	0.92	122.5	1.4	0.4	4.5	50.6 \pm 0.4	52.6	
42-A		1.71	350	12.26	100–475	12	0.61	0.90	41.0	1.8	2.0	6.5	51.9 \pm 0.7	50.9	
43-B		1.68	474	8.90	100–500	13	0.70	0.88	33.2	2.2	1.2	7.1	61.6 \pm 1.1	58.8	
44-A		3.31	1070	7.78	100–450	11	0.53	0.89	11.5	3.9	1.1	9.3	62.1 \pm 2.6	61.9	
45-B		1.91	584	8.24	100–550	15	0.79	0.92	44.9	2.1	1.6	4.6	53.4 \pm 0.9	54.5	
46-A		2.50	880	7.13	100–375	8	0.73	0.83	15.6	2.0	1.3	4.7	60.2 \pm 2.2	58.3	
47-B		0.79	192	10.36	100–600	17	0.89	0.92	131.8	2.3	2.5	6.0	52.7 \pm 0.4	52.5	
48-A		4.35	613	17.84	100–525	14	0.84	0.90	38.0	2.1	1.4	6.9	57.3 \pm 1.2	56.9	
49-A		0.52	109	11.99	100–600	17	0.91	0.92	95.8	2.9	0.4	5.5	52.5 \pm 0.5	52.7	
50-A		4.03	707	14.31	100–425	10	0.66	0.86	18.9	3.1	1.9	11.0	62.1 \pm 1.9	62.3	
52-A		3.73	677	13.85	100–550	15	0.85	0.91	73.1	2.1	0.7	6.1	59.5 \pm 0.6	58.1	
53-B		3.98	1020	9.81	100–525	14	0.74	0.92	27.4	2.2	1.3	7.4	53.9 \pm 1.3	52.8	
54-A		2.83	594	11.99	100–550	15	0.85	0.92	60.6	1.3	0.9	3.5	54.2 \pm 0.7	52.6	
55-A	3.04	822	9.28	100–475	12	0.60	0.90	14.9	4.2	1.4	7.2	52.5 \pm 1.9	50.4		
56-A	7.68	1274	15.14	100–425	10	0.74	0.87	33.6	2.0	0.1	6.3	62.9 \pm 1.2	60.6		
VALL 1575–1625	1-A	2.63	456	14.51	100–390	8	0.85	0.83	69.4	1.3	2.2	5.4	61.5 \pm 0.7	60.9	
	2-A	2.60	454	14.38	100–420	9	0.91	0.83	26.8	2.3	3.0	5.3	54.5 \pm 1.5	55.4	
	3-A	2.73	481	14.28	100–420	9	0.90	0.82	46.2	1.2	0.1	2.7	59.3 \pm 1.0	59.7	
	4-A	4.47	669	16.79	100–420	9	0.90	0.83	74.0	1.2	0.4	2.0	57.3 \pm 0.6	56.3	
	5-A	2.04	293	17.52	100–420	9	0.90	0.83	88.0	1.5	1.1	4.6	58.7 \pm 0.5	58.1	

Table 2. (continued)

Name (Age)	Sample Number	NRM (A/m)	χ (10^{-5})	Q	$T_{\min}-T_{\max}$ ($^{\circ}\text{C}$)	n	f	g	q	MAD ($^{\circ}$)	DANG ($^{\circ}$)	CRM (%)	$F \pm \sigma F$ (μT)	F_c (μT)
	7-A	1.45	272	13.38	100–420	9	0.70	0.86	38.7	4.5	1.9	4.1	56.8 ± 0.9	55.2
	8-A	1.13	236	11.99	100–390	8	0.86	0.84	47.8	1.0	3.8	8.8	48.3 ± 0.8	47.8
	14-A	2.87	503	14.33	100–420	9	0.92	0.84	33.1	1.5	0.4	3.7	55.9 ± 1.3	57.2
	16-A	3.65	852	10.77	100–390	8	0.84	0.83	19.1	3.1	3.2	8.1	53.3 ± 1.8	51.7
	17-A	2.70	1429	4.75	100–390	8	0.73	0.83	18.2	2.8	1.7	6.4	50.7 ± 1.7	50.9
	18-A	3.93	518	19.07	100–390	8	0.89	0.79	50.6	2.1	3.0	5.0	55.6 ± 0.8	57.6
Bricks GUA2	3-A	0.23	283	2.0	100–560	12	0.82	0.90	67.4	2.3	0.7	2.6	48.2 ± 0.5	44.3
1825–1845	4-A	2.34	184	32.0	100–400	8	0.80	0.85	59.9	1.7	0.9	0.8	49.3 ± 0.5	46.7
	6-A	3.22	744	10.9	100–470	10	0.84	0.88	37.0	2.1	0.7	1.6	49.2 ± 1.0	45.6
	7-A	0.15	30	12.6	100–600	15	0.85	0.91	116.7	1.9	1.6	4.5	53.7 ± 0.4	50.2
	8-A	0.19	123	3.9	100–530	12	0.79	0.88	67.0	3.0	1.3	1.5	53.8 ± 0.5	46.7
	9-A	7.59	659	28.9	100–400	8	0.83	0.83	68.2	0.9	0.5	1.3	49.9 ± 0.5	48.4
YUS2	11A3	0.14	17	20.7	100–580	14	0.62	0.85	12.80	1.7	1.1		43.3 ± 1.9	
1959	13A3	0.15	23	16.4	100–580	14	0.99	0.86	27.70	4.8	3.1		43.3 ± 1.3	
	23A1	0.8	86	23.4	100–560	13	0.90	0.83	151.80	0.8	0.1		53.8 ± 0.3	53.8
	41A2	0.8	47	42.8	100–530	12	0.92	0.74	25.25	2.9	2.6	3.8	44.1 ± 0.8	41.7
	43A3	13	888	36.8	100–530	12	0.99	0.87	43.36	3.3	2.5	2.6	42.0 ± 0.9	41.0

^aName (Age), name of the group samples (age of the samples); NRM, intensity of the natural remanent magnetization in A/m; χ , initial susceptibility in 10^{-5} SI units; Q , Koenigsberger ratio for an ambient magnetic field of $50 \mu\text{T}$; interval temperature $T_{\min}-T_{\max}$ used for the slope calculation; n , number of data points within this temperature interval; f , fraction of the NRM component used in the slope calculation; g , gap factor; q , quality factor; MAD, maximum angle of deviation; DANG, deviation angle; CRM, potential error on the estimation of the paleointensity due to the acquisition of CRM during Thellier experiment as a percentage of the applied field; $F \pm \sigma F$, paleointensity estimate and its standard error without anisotropy correction; F_c , paleointensity estimate after correction of anisotropy.

to multidomain (MD) pure magnetite grains [McClelland Brown, 1984]. In our samples there is no evidence for MD grain behavior since curvature in the NRM/TRM plots is not seen. The linearity of these diagrams clearly indicates the dominance of single-domain (SD) magnetic grains. Our samples are characterized by Curie temperatures lower than 580°C , suggesting that the magnetic carriers are not pure magnetite.

[22] A linear cooling time of 48 h was also applied. A very small increase in the correction factors was observed. For this reason, and in order to retain the mean intensity values least affected by magnetochemical alteration, we consider that the mean intensity values corrected for a cooling time of 24 h are the most reliable.

5.5. New Archeointensity Results

[23] Seventeen new mean archeointensity determinations have been obtained. The standard deviation around the mean intensity (s.d.) is lower than 8% for 9 of them (Table 3 and Figure 11a). For 5 sites s.d. is between 8 and 11%, and for the other three (CERCALB, YUS2 and MURG) the s.d. is greater, between 11 and 18%. Archeointensity values determined from sites dated within the same time interval are generally close, for example VALN and VALI or VALM and CALC. The results obtained for the kiln CALB are very similar to the result obtained for the group of jar fragments CERCALB fired within this kiln. However, the mean intensity from CALA (dated at the same interval as CALB) is $4 \mu\text{T}$ (6%) higher. The archeological constraints clearly indicate that the kilns CALA and CALB, sampled at the same archeological site, are contemporaneous and dated between 1275 and 1300 AD [Gómez-Paccard et al., 2006b]. The very similar archeomagnetic directions for CALA and CALB (Table 1 and Figure 3) obtained are in agreement with the archeological information. This indicates that the differences observed are most probably related to the precision limit of the archeointensity determinations [Gómez-Paccard et al., 2006a]. The slight differences seen between mean

intensity from other contemporaneous kilns may be partially explained by the kilns being different ages (inside the interval proposed by archeologists) or again, may reflect the limitations of the experimental method and/or samples [Gómez-Paccard et al., 2006a].

6. Mean Archeointensity Curve and Discussion

6.1. Archeointensity Results for Western Europe Over the Last 2000 Years

[24] Chauvin et al. [2000] compiled available results for western Europe giving different weights to the data in order to reduce the considerable scatter seen. The data were weighted depending on three criteria: the paleointensity technique used, the type of materials analyzed and the number of samples per site used to calculate the mean. Chauvin et al. [2000] demonstrated that some of the available results (associated with low weighting factors) do not seem to be reliable. Therefore, we have conducted the same analysis and compiled here the most reliable data from western Europe. The compilation has been restricted to the past two millennia and to sites for which the weight was equal or bigger than 10 (the maximum weight possible is 16 and the minimum is 3). The retained data, coming from Spain, France, Denmark and South Norway, are described in the following paragraphs.

6.1.1. Spain

[25] There are only 8 previously published archeointensity data from Spain with a weight equal or bigger than 10 for the last two millennia. The first one, obtained from a Roman pottery kiln has been published by Kovacheva et al. [1995]. Recently, seven archeointensity values were obtained from contemporaneous kilns from Murcia dated between 1100 and 1200 AD by archeological constraints [Gómez-Paccard et al., 2006a]. These data were obtained using the classical Thellier method and were corrected for TRM anisotropy and cooling rate effect using a cooling time of 24 h.

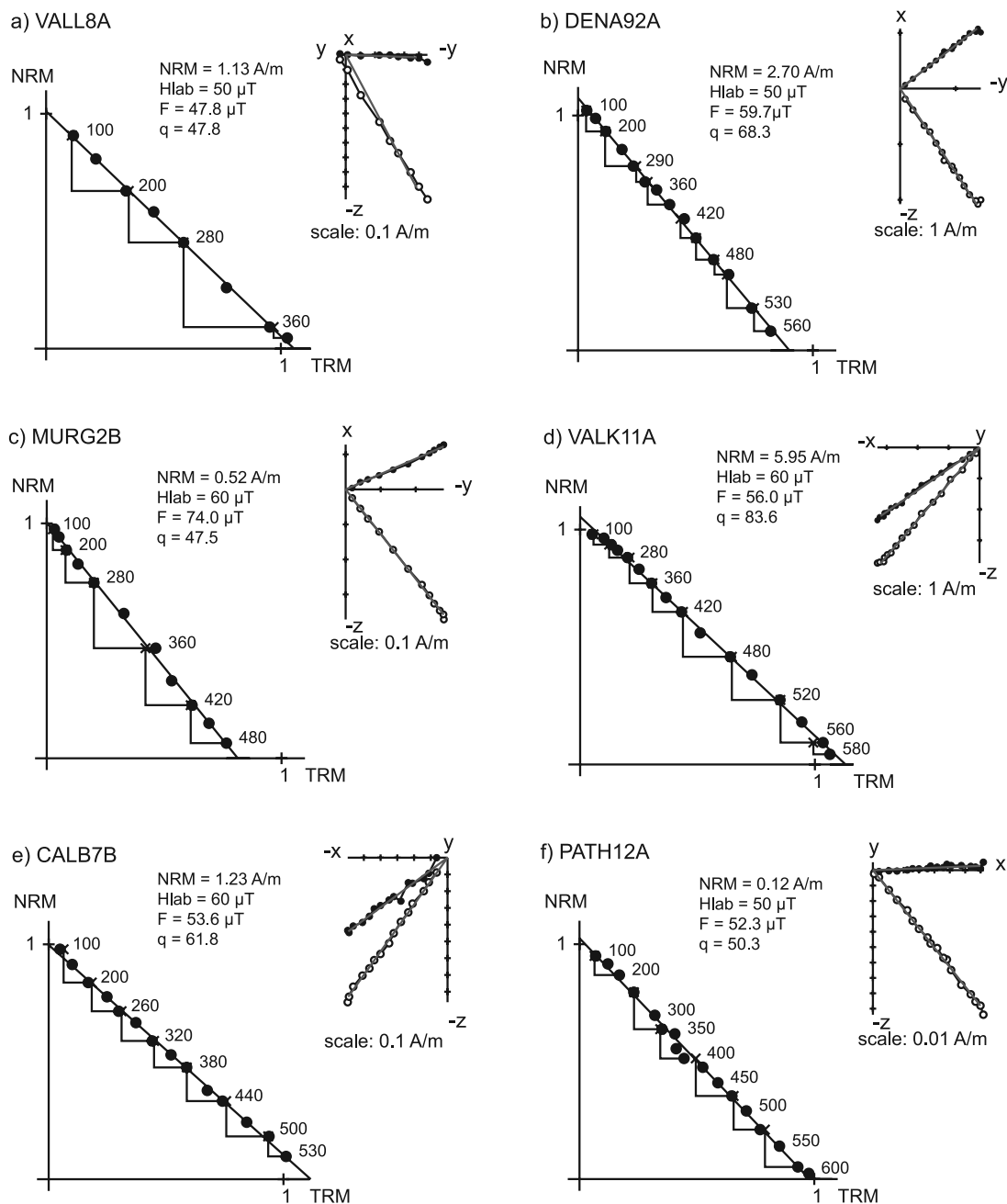


Figure 7. Examples of single component natural remanent magnetization/thermoremanent magnetization (NRM/TRM) diagrams together with orthogonal vector projections of the remanent magnetization in sample coordinates. Open (solid) circles are projections upon vertical (horizontal) planes. Diagrams are normalized to the initial NRM intensity. Closed circles on the NRM/TRM diagrams are data used for archeointensity determinations. The laboratory field (Hlab) used during the Thellier experiments and the obtained paleointensity (F) together with the quality factor q are indicated.

6.1.2. France

[26] Data published by *Gallet et al.* [2005], *Genevey and Gallet* [2002] and *Chauvin et al.* [2000] were acquired by the Thellier method and corrected for TRM anisotropy and cooling rate effects. Different cooling times were used to correct the archeointensity means. For this region 41 high-quality archeointensity results for the last two millennia are available.

6.1.3. Denmark and South Norway

[27] *Gram-Jensen et al.* [2000] studied 15 archeomagnetic sites in Denmark and one in South Norway. The experiments were performed using the Thellier method, and TRM anisotropy was investigated. However, no cooling rate corrections were performed in this study. Although the number of samples is low for some sites and no cooling rate corrections were performed, 13 paleointensity values satisfied our criteria [*Chauvin et al.*, 2000, 2005].

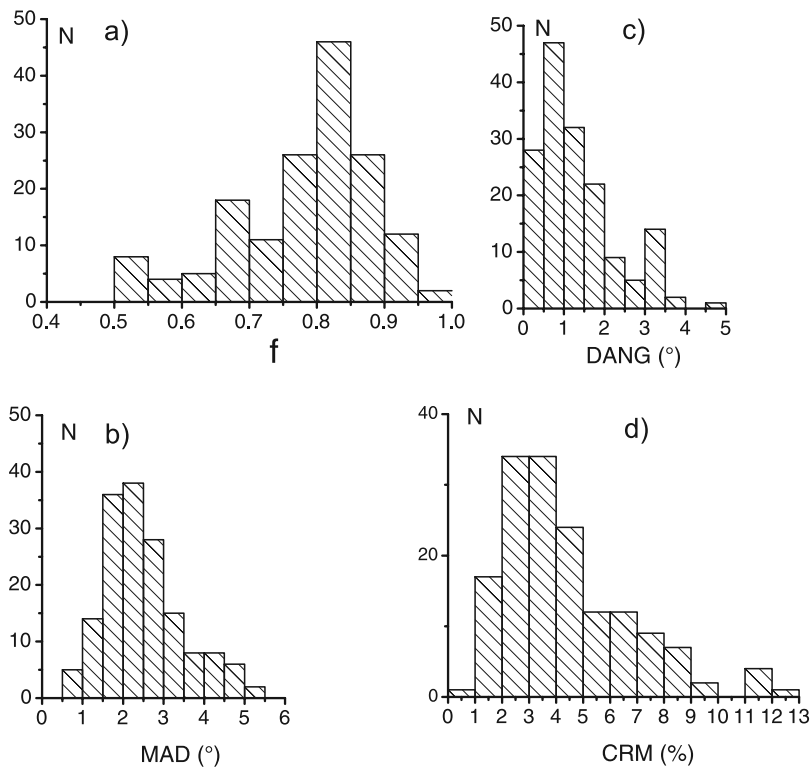


Figure 8. Variations of some parameters used to test the quality of our archeointensity determinations. (a) f , fraction of the NRM component used in the slope calculation; (b) MAD, maximum angle of deviation; (c) DANG, deviation angle and (d) CRM, potential error on the estimation of the paleointensity due to the acquisition of chemical remanent magnetization as a percentage of the applied field.

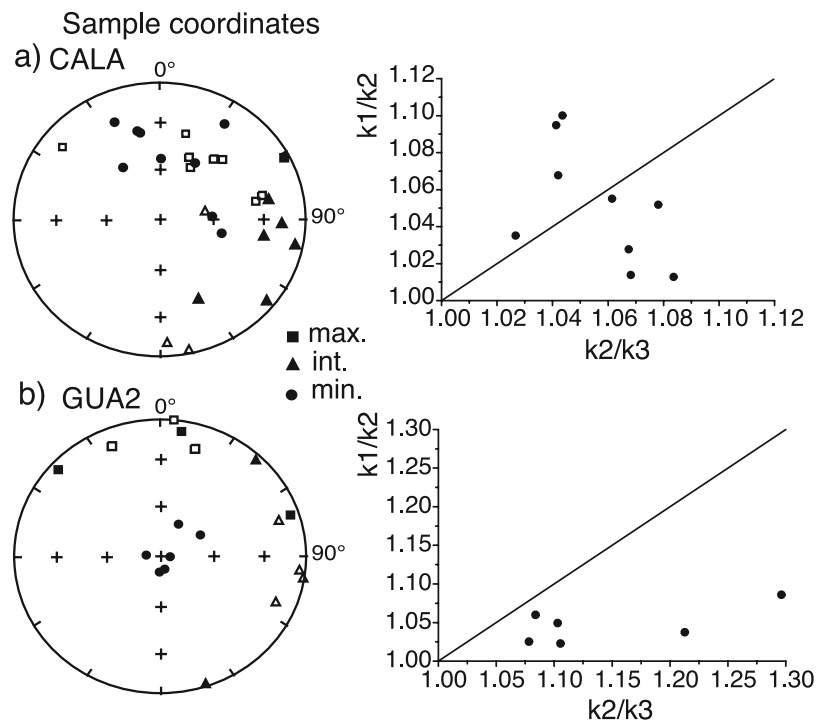


Figure 9. Examples of stereographic projections of the direction of the principal axes of the TRM anisotropy tensor, and Flinn diagrams of individual sample lineation and foliation data for (a) kiln CALA and (b) bricks from GUA2. Results are plotted in sample coordinates. Samples were drilled perpendicularly to the flattening plane of the samples (when present).

Table 3. Archeointensity Results per Structure or Group of Samples^a

Name	Age (years AD)	N/N _O	$F_m \pm \text{s.d.}$ (μT)	F_{po} (μT)	F_{pocr} (μT)	F_{pa} (μT)	VDM 10^{22} A/m^2	VADM 10^{22} A/m^2
DENA	220–250	10/10	59.0 \pm 3.1	58.8	54.4 \pm 3.4	61.1	10.2	9.5
MURG	1000–1100	8/8	55.5 \pm 9.6	58.0	58.3 \pm 10.5	66.4	11.1	10.3
CALA	1275–1300	9/9	59.9 \pm 2.8	59.3	58.4 \pm 3.1	66.8	12.0	10.2
CALB	1275–1300	10/12	56.6 \pm 4.2	56.4	54.4 \pm 3.7	62.2	11.2	9.5
CERCALB	1275–1300	4/5	54.6 \pm 7.0	55.9	55.6 \pm 7.0	61.8	11.4	9.7
VALN	1238–1350	11/12	50.4 \pm 3.1	50.7	48.5 \pm 2.6	54.7	9.7	8.4
VALI	1238–1400	11/11	54.4 \pm 3.1	54.6	50.4 \pm 2.0	57.9	10.2	8.8
VALK	1300–1450	9/9	54.9 \pm 3.6	55.4	51.6 \pm 4.1	58.3	10.6	9.0
VALM	1300–1450	9/9	49.9 \pm 4.3	49.9	47.1 \pm 4.5	53.2	9.4	8.2
CALC	1400–1420	9/9	50.3 \pm 2.5	50.2	48.7 \pm 3.0	53.3	9.7	8.5
PATH	1450–1600	10/11	55.5 \pm 4.3	54.4	52.5 \pm 5.3	58.7	9.8	9.1
PATA	1450–1500	10/12	51.8 \pm 4.9	52.7	51.2 \pm 5.3	56.9	9.2	8.9
PATB	1525–1650	12/13	51.9 \pm 4.2	50.6	50.4 \pm 4.0	55.1	8.2	8.8
PATJ	1429–1611	16/17	55.5 \pm 4.0	54.5	52.5 \pm 4.2	57.6	8.7	9.1
VALL	1575–1625	11/13	55.5 \pm 4.0	56.4	55.4 \pm 4.6	61.1	9.9	9.6
Bricks GUA2	1825–1845	6/10	47.0 \pm 2.1	47.4	46.8 \pm 2.9	51.0	7.9	8.0
YUS2	1959	5/5	45.3 \pm 4.8	49.2	48.1 \pm 6.5	52.8	8.4	8.3

^aName, name of the structure or group of samples; Age, age of the structure; N/N_O number of accepted/number of studied samples; $F_m \pm \text{s.d.}$, anisotropy corrected mean intensity and standard deviation; F_{po} , weighted mean intensity; F_{pocr} , weighted mean intensity after cooling rate correction, F_{pa} , weighted mean intensity at the latitude of Paris after cooling rate correction; VDM and VADM, values of the virtual dipole moment and virtual axial dipole moment calculated using the weighted mean intensities corrected for the effect of cooling rate upon TRM acquisition.

[28] The 17 new Spanish data together with the previous results for France, Spain, Denmark and South Norway are shown in Figure 11a. The centered dipole moment model was used to calculate the paleointensities at the latitude of Paris. This relocation process may introduce some errors, which can be estimated using the IGRF 2000 model. Murcia, the most distant locality from Paris in our data set was chosen to conduct this test. The difference between the relocated intensity and the direct intensity at Paris is 3 μT (6%). This discrepancy is of the same order or lower than the typical error associated with the compiled mean paleointensity data (see Figure 11a or Table 3). As there is no way to quantify relocation error systematically we do not take them into account.

[29] During the 3rd, the 14th and the 16th centuries our new Spanish intensity data are in very good agreement with the other results (see Figure 11a). For the modern periods, we note that the mean intensity of YUS2 (48.1 \pm 6.5 μT) is in agreement with the IGRF at Yuste for 1959 AD (43.8 μT) if we take into account the s.d. around the mean value. In contrast, some discrepancies are observed for other periods. For example, the three data from Calatrava, around 1250 AD (sites CALA-B) differ by 10 μT or more from the previous results obtained by *Genevey and Gallet* [2002]. It is worth pointing out that some dispersion of the data is generally observed for all the periods covered (Figure 11a), both between data published by the same authors, or between data acquired by different laboratories. Some of the scatter may be due to age uncertainties. However, even for contemporaneous structures, sampled at the same archeological site and carrying very close directions of magnetization (as data from *Gómez-Paccard et al.* [2006a] or CALA-B), the dispersion in the intensity data is seen. The same fact is also observed in other studies [*Hill et al.*, 2007]. Therefore, some part of the dispersion is probably an indication of the limitations of the experimental method and/or the samples. This can include discrepancies between the true cooling time of the archeomagnetic structures and the cooling rate used in the laboratory. We can notice that the data are either not corrected [*Gram-Jensen et al.*, 2000] or corrected for the

cooling rate effect using 4 h [*Kovacheva et al.*, 1995], 8 h [*Chauvin et al.*, 2000], 10 or 33 h [*Gallet et al.*, 2005; *Genevey and Gallet*, 2002] or 24 h (this study) of cooling.

[30] The compiled data set includes several results per century, except for the period between 500 AD and 1100 AD. Future archeointensity research should focus on this period.

6.2. Evolution of the Geomagnetic Field Intensity in Western Europe Over the Past 2000 Years Inferred From Bayesian Modeling

[31] Bayesian modeling [*Lanos*, 2004] based on roughness penalty has been used in order to calculate the evolution of the geomagnetic intensity in western Europe during the last millennia. This approach puts some prior knowledge on the global nature of the curve to be estimated (it is assumed that the studied physical phenomena varies in a smooth way). It allows the window width to be automatically adapted to the density of points along the time axis, making the points movable inside the dating ranges; and it can take into account stratigraphic constraints provided by archeological investigations. Figure 11 shows the obtained curve together with the 95% error envelope at the latitude of Paris. Table 4 gives the results in 25-year steps. It is worth pointing out that the Bayesian curves computed with or without the data from Denmark and South Norway are very similar. This suggests that in this case the use of these data (not corrected for the cooling rate effect) do not introduce a significant bias.

[32] The results obtained using the classical moving average window technique have been also computed. In order to determine the best window widths to use, several values were tested (80, 100 and 120 years). No significant differences were found therefore it was decided to use a window width of 100 years, plotted in 25 years, with at least three reference points per window. The mean values obtained with the two methods (Bayesian and moving average window) are very similar (Figure 11b), although the moving window curve is not continuous because some time windows contain less than three archeointensity data.

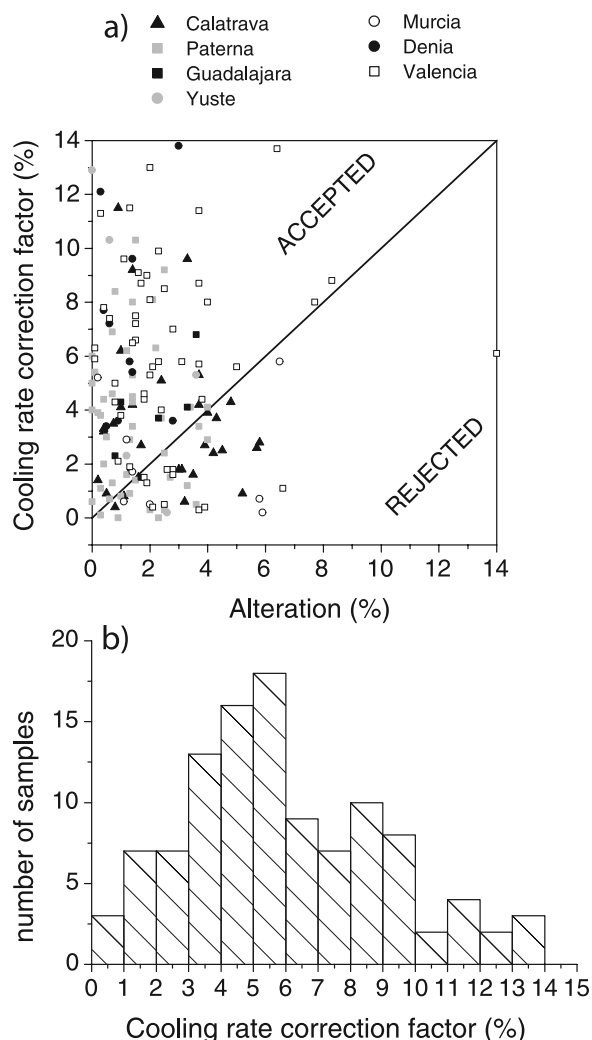


Figure 10. (a) Absolute values of the effect of cooling rate upon TRM intensity per sample versus the corresponding alteration (variation of the TRM acquisition capacity), for cooling times of 24 h, (b) histogram showing the cooling rate correction factors applied per sample.

[33] The Bayesian results, which take into account both uncertainties on ages and magnetic data, indicate small variations of the geomagnetic field intensity during Roman times (–200 to 400 AD). For High Middle Ages (around 600–900 AD) rapid variations ($7 \mu T$ per century) of the field strength have been proposed [Genevey and Gallet, 2002]. However, only three archeointensity data are available for this period and consequently, the Bayesian curve is not very well constrained. The smaller narrow bump in intensity proposed by Genevey and Gallet [2002] during the 14th and 15th centuries is not confirmed by our results. On the contrary, the geomagnetic field intensity seems to be constant between the 14th and the 16th centuries, before decreasing from $56 \mu T$ to $47 \mu T$ during the 17th and 18th centuries. The Bayesian curve has been compared with direct measurements made near Paris (Figure 11a). The fit between the curve and direct measurements seems good for the 19th century. This indicates a small overestimation of the field intensity during the 20th century.

[34] Recent analysis showed that secular variation in western Europe is characterized over the last two millennia, by two major directional changes at 200, and 1350 AD [Gómez-Paccard et al., 2006c]. Neither of these cusps seems clearly associated with a large intensity increase (see Figure 11).

[35] Recently, Gallet et al. [2005] and Courtillot et al. [2007] proposed a connection between the geomagnetic field and climate changes over centennial timescales. These authors found within their French archeointensity data a relationship between rapid intensity increases and the occurrence of cooling periods in western Europe for the last two millennia. The western European data compiled here (Figure 11), as well as the Bayesian and moving window average obtained in this work, do not clearly show all the intensity peaks proposed by Gallet et al. [2005] which were used for comparison with climatic changes.

[36] One cannot reject the suggestion that the Bayesian treatment or moving window average used in this work can lead to a too smoothed mean curve. However, as previously discussed, scatter of the order of 10% might be caused by errors in age and limitations of the experimental method and/or samples. This scatter has to be taken into account in the analysis [McElhinny and Senanayake, 1982; Korte and Constable, 2005b]. This can be achieved by obtaining a larger number of archeointensity data for each time interval, as has been done for directional secular variation curves [Gallet et al., 2002; Schnepf and Lanos, 2005; Gómez-Paccard et al., 2006c] and by using an accurate method for the computation of the mean curve. We clearly need more high-quality data in order to refine the variation of the geomagnetic field intensity for western Europe. Only with a refined curve will it become possible to test rigorously the hypothesis (still discussed, see Bard and Delaygue [2008] and Courtillot et al. [2008]) of a connection between the Earth's magnetic field and climate at this timescale.

[37] The Bayesian intensity curve proposed here has been compared with the CALS3(7)K.2 global models of Korte and Constable [2005a], the model of Hongre et al. [1998] and the GUFM1 model of Jackson et al. [2000]. The fit between the prediction of the CALS3(7)K.2 model and our curve seems very good (Figure 12). The prediction is practically contained inside the Bayesian error margin at 95% confidence level. The similarity of the curves could be explained by the fact that the majority of the archeointensity data used in CALS3(7)K.2 are European. In contrast the intensity predictions obtained with Hongre's model are not so similar to the curve obtained. This model shows, in general, higher values than the Bayesian curve (see Figure 12).

6.3. Dipole Moment and Comparison With Global Models

[38] Figure 13 shows the variation curve of the virtual axial dipole moments (VADM) for eastern Europe [Valet, 2003] and the VADM Bayesian curve obtained using the western European data compiled in this work. Since European archeomagnetic data do not always incorporate inclination records, comparison must rely on VADMs. The eastern European curve indicates a more significant intensity variation at a shorter timescale than our western European curve (Figure 13). Korte and Constable [2006]

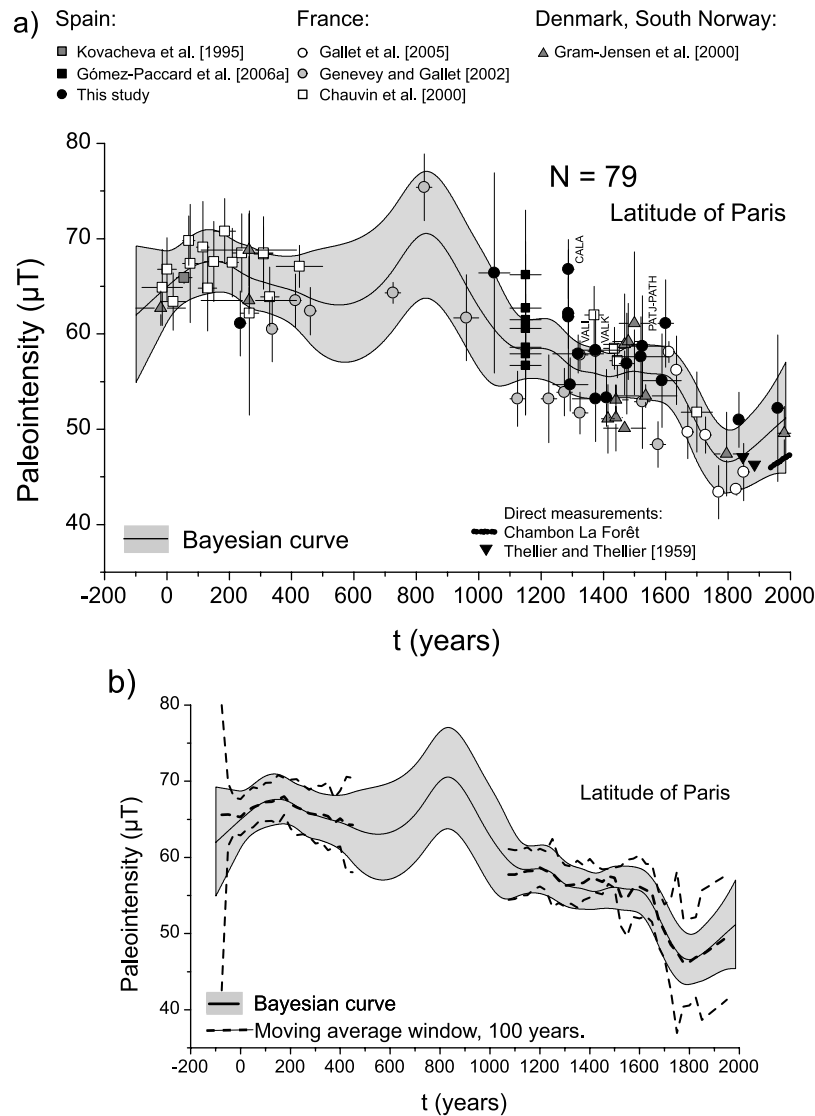


Figure 11. (a) Evolution of the geomagnetic intensity obtained by Bayesian modeling. The mean curve is shown together with the marginal errors at 95% confidence level. The 79 reliable paleointensity data for western Europe used are plotted together with direct measurements made in Paris [Thellier and Thellier, 1959] and at Chambon La Forêt observatory, near Paris (Bureau Central du Magnétisme, <http://obsmag.ipgp.jussieu.fr/>, <ftp://par-gin.ipgp.jussieu.fr/BcmtDataBase/clf/clf.year>), and (b) comparison between the Bayesian and the moving average window curve obtained using a window width of 100 years. All at the latitude of Paris.

suggest that over the last 7 ka, phases of true dipole decrease or increase could be decadal to centennial in length, as it is observed over the last 150 years by direct measurements. So some parts of the small timescale variations observed in Figure 13 could reflect a true dipole moment variation. Differences observed between eastern and western European curves could be related to the type of methods used for their construction (stacking of three curves built by moving window averages of data from Bulgaria, Caucasus and Ukraine in the first case, and the Bayesian method in the second case). They could be explained also by the lack of data for some periods, or by some small geographical length-scale nondipole effects.

[39] Dipole moments calculated using GUFM1, CALS3(7)K.2 and Hongre et al. [1998] spherical harmonic

analysis (SHA) global models, together with the estimation of the dipole moment published by Gubbins et al. [2006] and the VADMs obtained by Yang et al. [2000] and Valet et al. [2008] from archeomagnetic data are also shown in Figure 13. The dipole moment values estimated by these different works are in close agreement for the last three or four centuries.

[40] In the contrary, some discrepancies are observed before 1500 AD or for older periods. The dipole moment obtained by Hongre et al. [1998] model fits better the VADM results published by Yang et al. [2000], Valet [2003] or Valet et al. [2008] than the dipole moment obtained by CALS3(7)K.2 models. VADMs published by Yang et al. [2000] and by Valet et al. [2008] were obtained using global compilations of archeointensity data. Then, they are supposed to eliminate the nondipole component of the Earth's

Table 4. Intensity Curve Obtained by Bayesian Modeling Each 25 Years^a

Age	F (μT)	Error Min.	Error Max.	Age	F (μT)	Error Min.	Error Max.
-100	61.98	54.92	69.24	950	65.69	59.17	72.26
-75	62.71	56.45	69.11	975	64.21	57.71	70.77
-50	63.46	58.04	68.97	1000	62.83	56.36	69.35
-25	64.21	59.63	68.83	1025	61.59	55.29	67.90
0	64.96	61.19	68.73	1050	60.49	54.66	66.35
25	65.66	62.37	68.97	1075	59.56	54.55	64.68
50	66.34	63.14	69.55	1100	58.87	54.77	63.14
75	66.93	63.63	70.20	1125	58.48	55.09	62.03
100	67.32	63.95	70.68	1150	58.42	55.29	61.56
125	67.55	64.18	70.93	1170	58.47	55.35	61.51
150	67.63	64.35	70.91	1200	58.50	55.26	61.61
175	67.54	64.40	70.61	1225	58.35	55.02	61.56
200	67.21	64.24	70.12	1250	57.92	54.63	61.12
225	66.71	63.79	69.65	1275	57.19	54.12	60.31
250	66.22	63.13	69.35	1300	56.53	53.66	59.52
275	65.82	62.62	69.05	1325	56.15	53.38	58.98
300	65.54	62.40	68.68	1350	56.00	53.25	58.69
325	65.29	62.19	68.39	1375	55.85	53.20	58.43
350	65.05	61.90	68.24	1400	55.61	53.17	58.11
375	64.84	61.52	68.16	1425	55.54	53.21	57.95
400	64.60	61.00	68.17	1450	55.72	53.30	58.16
425	64.29	60.24	68.30	1475	55.99	53.31	58.58
450	63.91	59.31	68.54	1500	56.08	53.25	58.83
475	63.56	58.46	68.78	1525	55.97	53.12	58.88
500	63.29	57.81	68.97	1550	55.85	53.05	58.85
525	63.12	57.35	69.15	1575	55.80	52.95	58.78
550	63.05	57.10	69.33	1600	55.66	52.64	58.58
575	63.10	57.04	69.54	1625	55.04	51.76	58.12
600	63.29	57.16	69.82	1650	53.84	50.31	57.25
625	63.63	57.46	70.20	1675	52.26	48.48	56.01
650	64.12	57.94	70.69	1700	50.55	46.62	54.51
675	64.79	58.59	71.33	1725	48.93	45.12	52.83
700	65.65	59.40	72.15	1750	47.64	44.01	51.40
725	66.70	60.38	73.18	1775	46.83	43.40	50.40
750	67.91	61.47	74.38	1800	46.59	43.33	49.93
775	69.10	62.52	75.57	1825	46.81	43.53	50.08
800	70.04	63.34	76.53	1850	47.32	43.78	50.76
825	70.52	63.75	77.03	1875	47.96	44.15	51.62
850	70.38	63.59	76.91	1900	48.67	44.60	52.58
875	69.68	62.93	76.22	1925	49.42	45.02	53.68
900	68.57	61.90	75.13	1950	50.17	45.32	54.95
925	67.19	60.61	73.76	1975	50.90	45.39	56.42

^aAge, age in years; F , intensity in μT ; error min. and error max., minimum and maximum marginal errors in μT . All data at the latitude of Paris.

magnetic field. It seems that the Korte and Constable models underestimate the dipole part of the Earth's magnetic field for some time periods.

[41] Discrepancies between VADM (or VDM) data and dipole moment computed from SHA have already been recognized [Korte and Constable, 2005b]. The authors suggested that VADM (or VDM) averaged over centennial and millennial timescales are higher than the true dipole moment. They attributed the bias observed in VADM (VDM) data to an incomplete average of the nondipole field and to data quality.

[42] As VADM curves computed from one site (western or eastern Europe) do not completely remove contributions from the nondipole field, their analysis suggests that the nondipole part of the field over Europe was important at some periods, for example during the two first centuries or between 600 and 900 AD (see Figure 13). Note that during these periods the intensity predictions (using CALS3(7)K.2 models) at Paris agree very well with our obtained curve (see Figure 12).

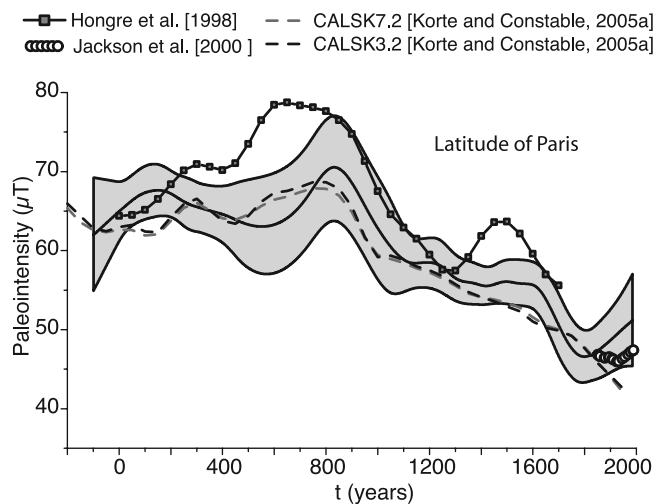


Figure 12. Comparison between the intensity Bayesian curve and global models. All at the latitude of Paris.

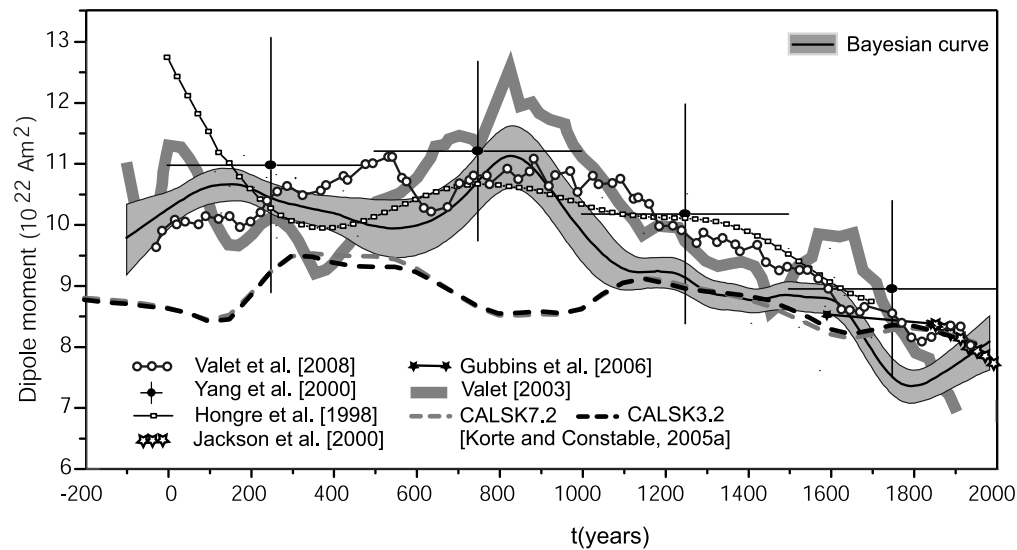


Figure 13. Comparison between dipole moment predicted by global models, time-averaged virtual axial dipole moments (VADM) results from *Yang et al.* [2000] and *Valet et al.* [2008], the dipole moment curve for eastern Europe from *Valet* [2003], and the dipole moment evolution proposed in this work inferred from Bayesian modeling and the most reliable western European data.

[43] However, discrepancies between VADM computed using data from different locations around the world and dipole moment computed from CALS(3)7K.2 models could also be explained by a lack of power in the dipole term of this SHA [*Valet et al.*, 2008].

[44] In our opinion, strong geographical biases in the distribution of the data seem to affect both VADM (VDM) average results and dipole moment variations computed from SHA. An increase of the number of archeointensity data and a better geographical distribution of them are clearly needed in order to better constrain the accuracy of global models.

7. Conclusions

[45] Seventeen new mean archeointensity determinations have been obtained on kilns and large jar fragments, with standard deviation (s.d.) lower than 8% for 9 of the 17 sites. Our new data, together with 62 previous results from France, Denmark and Spain, have been used to construct a geomagnetic field intensity variation curve for western Europe. Bayesian modeling was used for this purpose. The intensity curve obtained using the classical moving average method gives very similar results. Geomagnetic field intensity remained more or less constant between the 1st and 4th centuries, and between the 14th and 16th centuries (mean values around 65 and 57 μT , respectively), whereas an important decrease occurs between the 17th and 18th centuries. More data are clearly needed in order to establish a reliable reference curve for High Middle Ages (600–1000 AD).

[46] Differences between geomagnetic global models [*Hongre et al.*, 1998; *Korte and Constable*, 2005a], and between these models and VADMs [*Yang et al.*, 2000; *Valet et al.*, 2008] have been observed. This indicates the need to obtain more reliable archeointensity data and to improve the geographical sites distribution. Our work also indicates that errors in ages and limitations in experimental method and/or

the samples have to be taken into account before testing the hypothesis of a relationship between field intensity and climate changes over the last millennia [*Gallet et al.*, 2005; *Courtillot et al.*, 2007].

[47] The new data enhance the European data set. The use of the intensity reference curve obtained for dating remains very difficult for some periods because of little variation of the geomagnetic field or to the large envelope error of the curve. However, for some periods and for displaced objects, the intensity curve proposed should be useful for future archeomagnetic dating in this region.

[48] **Acknowledgments.** Sincere thanks are given to I. García-Villanueva, J. A. Gisbert-Santonja, M. A. Hervás, P. Jiménez-Castillo, M. Mesquida-García, and M. Retuerce for their important role in this study; without their archeological help this research would not be possible. Thanks are due to M. Hill for her careful reading of this manuscript. We are grateful to M. Kovacheva and M. Korte for their constructive reviews of this paper. This study is part of the Archeomagnetic Applications for the Rescue of the Cultural Heritage (AARCH) project, contract HPRN-CT2002-00219. Additional funding has also been provided by the Spanish Ministerio de Ciencia y Tecnología (project CGL2005-00211/BTE and the “Juan de la Cierva” Fellowship Programme).

References

- Bard, E., and G. Delaygue (2008), Comment on “Are there connections between the Earth’s magnetic field and climate?” by V. Courtillot et al. [*Earth and Planetary Science Letters*, 253, 328, 2007], *Earth Planet. Sci. Lett.*, 265(1–2), 302–307, doi:10.1016/j.epsl.2007.09.046.
- Batt, C. (1997), The British archaeomagnetic calibration curve: An objective treatment, *Archaeometry*, 39, 153–168, doi:10.1111/j.1475-4754.1997.tb00795.x.
- Bucur, I. (1994), The direction of the terrestrial magnetic field in France during the last 21 centuries: Recent progress, *Phys. Earth Planet. Inter.*, 87(1–2), 95–109, doi:10.1016/0031-9201(94)90024-8.
- Burakov, K. S., I. E. Nachasova, T. Najera, F. Molina, and H. Cámara (2005), Geomagnetic intensity in Spain in the second millennium BC, *Izv. Russ. Acad. Sci. Phys. Solid Earth, Engl. Transl.*, 41(8), 622–633.
- Burakov, K. S., I. E. Nachasova, and C. Mata (2006), Geomagnetic field intensity in the first millennium BC from data on ceramics of the Los Villares archaeological monument (Spain), *Izv. Russ. Acad. Sci. Phys. Solid Earth, Engl. Transl.*, 42(11), 942–950.
- Chauvin, A., Y. Garcia, P. Lanos, and F. Laubenheimer (2000), Paleointensity of the geomagnetic field recovered on archaeomagnetic sites from France,

- Phys. Earth Planet. Inter.*, 120(1–2), 111–136, doi:10.1016/S0031-9201(00)00148-5.
- Chauvin, A., P. Roperch, and S. Levi (2005), Reliability of geomagnetic paleointensity data: The effects of the NRM fraction and concave-up behavior on paleointensity determinations by the Thellier method, *Phys. Earth Planet. Inter.*, 150(4), 265–286, doi:10.1016/j.pepi.2004.11.008.
- Courtillot, V., Y. Gallet, J. L. Le Mouél, F. Fluteau, and A. Genevey (2007), Are there connections between the Earth's magnetic field and climate?, *Earth Planet. Sci. Lett.*, 253(3–4), 328–339, doi:10.1016/j.epsl.2006.10.032.
- Courtillot, V., Y. Gallet, J. L. Le Mouél, F. Fluteau, and A. Genevey (2008), Response to comment on “Are there connections between Earth's magnetic field and climate?” by E. Bard and M. Delaygue [*Earth and Planetary Science Letters*, 253, 328–339, 2007], *Earth Planet. Sci. Lett.*, 265, 308–311, doi:10.1016/j.epsl.2007.09.031.
- Fisher, R. A. (1953), Dispersion on a sphere, *Proc. R. Soc. London, Ser. A*, 217, 295, doi:10.1098/rspa.1953.0064.
- Gallet, Y., A. Genevey, and M. Le Goff (2002), Three millennia of directional variation of the Earth's magnetic field in western Europe as revealed by archaeological artefacts, *Phys. Earth Planet. Inter.*, 131(1), 81–89, doi:10.1016/S0031-9201(02)00030-4.
- Gallet, Y., A. Genevey, and F. Fluteau (2005), Does Earth's magnetic field secular variation control centennial climate change?, *Earth Planet. Sci. Lett.*, 236(1–2), 339–347, doi:10.1016/j.epsl.2005.04.045.
- Genevey, A., and Y. Gallet (2002), Intensity of the geomagnetic field in western Europe over the past 2000 years: New data from ancient French pottery, *J. Geophys. Res.*, 107(B11), 2285, doi:10.1029/2001JB000701.
- Gómez-Paccard, M., A. Chauvin, P. Lanos, J. Thiriot, and P. Jiménez-Castillo (2006a), Archeomagnetic study of seven contemporaneous kilns from Murcia (Spain), *Phys. Earth Planet. Inter.*, 157(1–2), 16–32, doi:10.1016/j.pepi.2006.03.001.
- Gómez-Paccard, M., et al. (2006b), A catalogue of Spanish archaeomagnetic data, *Geophys. J. Int.*, 166(3), 1125–1143, doi:10.1111/j.1365-246X.2006.03020.x.
- Gómez-Paccard, M., A. Chauvin, P. Lanos, G. McIntosh, M. L. Osete, G. Catanzariti, V. C. Ruiz-Martínez, and J. I. Núñez (2006c), First archaeomagnetic secular variation curve for the Iberian Peninsula: Comparison with other data from western Europe and with global geomagnetic field models, *Geochem. Geophys. Geosyst.*, 7, Q12001, doi:10.1029/2006GC001476.
- Gram-Jensen, M., N. Abrahamsen, and A. Chauvin (2000), Archaeomagnetic intensity in Denmark, *Phys. Chem. Earth*, 25(5), 525–531, doi:10.1016/S1464-1895(00)00081-8.
- Gubbins, D., A. L. Jones, and C. C. Finlay (2006), Fall in Earth's magnetic field is erratic, *Science*, 312, 900–902, doi:10.1126/science.1124855.
- Hill, M., P. Lanos, A. Chauvin, D. Vitali, and F. Laubenheimer (2007), An archaeomagnetic investigation of a Roman amphorae workshop in Albinia (Italy), *Geophys. J. Int.*, 169(2), 471–482, doi:10.1111/j.1365-246X.2007.03362.x.
- Hongre, L., G. Hulot, and A. Khokhlov (1998), An analysis of the geomagnetic field over the past 2000 years, *Phys. Earth Planet. Inter.*, 106(3–4), 311–335, doi:10.1016/S0031-9201(97)00115-5.
- Jackson, A., A. R. T. Jonkers, and M. R. Walker (2000), Four centuries of geomagnetic secular variation from historical records, *Philos. Trans. R. Soc. London, Ser. A*, 358(1768), 957–990.
- Korte, M., and C. G. Constable (2005a), Continuous geomagnetic field models for the past 7 millennia: 2. CALS7K, *Geochem. Geophys. Geosyst.*, 6, Q02H16, doi:10.1029/2004GC000801.
- Korte, M., and C. G. Constable (2005b), The geomagnetic dipole moment over the last 7000 years—new results from a global model, *Earth Planet. Sci. Lett.*, 236(1–2), 348–358, doi:10.1016/j.epsl.2004.12.031.
- Korte, M., and C. G. Constable (2006), Centennial to millennial geomagnetic secular variation, *Geophys. J. Int.*, 167(1), 43–52, doi:10.1111/j.1365-246X.2006.03088.x.
- Korte, M., A. Genevey, C. G. Constable, U. Frank, and E. Schnepp (2005), Continuous geomagnetic field models for the past 7 millennia: 1. A new global data compilation, *Geochem. Geophys. Geosyst.*, 6, Q02H15, doi:10.1029/2004GC000800.
- Kovacheva, M., J. Parés, N. Jordanova, and V. Karlovovski (1995), A new contribution to the archaeomagnetic study of a Roman pottery kiln from Calahorra (Spain), *Geophys. J. Int.*, 123(3), 931–936, doi:10.1111/j.1365-246X.1995.tb06899.x.
- Kovacheva, M., N. Jordanova, and V. Karlovovski (1998), Geomagnetic field variations as determined from Bulgarian archaeomagnetic data. Part II: The last 8000 years, *Surv. Geophys.*, 19(5), 431–460, doi:10.1023/A:1006502313519.
- Lanos, P. (2004), Bayesian inference of calibration curves: Application to archaeomagnetism, in *Tools for Constructing Chronologies: Crossing Disciplinary Boundaries. Lecture Notes in Statistics*, edited by C. E. Buck and A. R. Millard, pp. 43–82, Springer, London.
- Lowrie, W. (1990), Identification of ferromagnetic minerals in a rock by coercivity and unblocking temperature properties, *Geophys. Res. Lett.*, 17(2), 159–162, doi:10.1029/GL017i002p00159.
- Márton, P. (2003), Recent achievements in archaeomagnetism in Hungary, *Geophys. J. Int.*, 153(3), 675–690, doi:10.1046/j.1365-246X.2003.01931.x.
- Márton, P., and E. Ferencz (2006), Hierarchical versus stratification statistical analysis of archaeomagnetic directions: The secular variation curve for Hungary, *Geophys. J. Int.*, 164(3), 484–489, doi:10.1111/j.1365-246X.2006.02873.x.
- McClelland Brown, E. (1984), Experiments on TRM intensity dependence on cooling rate, *J. Geophys. Res.*, 11, 205–208, doi:10.1029/GL011i003p00205.
- McElhinny, M. W., and W. E. Senanayake (1982), Variations in the geomagnetic dipole 1: The past 50 000 years, *J. Geomagn. Geoelectr.*, 34(1), 39–51.
- Nachasova, I. E., K. S. Burakov, and J. Bernabeu (2002), Geomagnetic field intensity variations in Spain, *Izv. Russ. Acad. Sci. Phys. Solid Earth, Engl. Transl.*, 38(5), 371–376.
- Nachasova, I. E., K. S. Burakov, F. Molina, and J. Cámara (2007), Archaeomagnetic study of ceramic from the neolithic Los Castillejos multilayer monument (Montefrío, Spain), *Izv. Russ. Acad. Sci. Phys. Solid Earth, Engl. Transl.*, 43(2), 170–176.
- Prévot, M., E. A. Mankinen, R. S. Coe, and C. S. Grommé (1985), The Steens Mountain (Oregon) geomagnetic polarity transition: 2. Field intensity variations and discussion of reversal models, *J. Geophys. Res.*, 90(B12), 10,417–10,448, doi:10.1029/JB090iB12p10417.
- Schnepp, E., and P. Lanos (2005), Archaeomagnetic secular variation in Germany during the past 2500 years, *Geophys. J. Int.*, 163(2), 479–490, doi:10.1111/j.1365-246X.2005.02734.x.
- Schnepp, E., and P. Lanos (2006), A preliminary secular variation reference curve for archaeomagnetic dating in Austria, *Geophys. J. Int.*, 166(1), 91–96, doi:10.1111/j.1365-246X.2006.03012.x.
- Tema, E., I. Hedley, and P. Lanos (2006), Archaeomagnetism in Italy: A compilation of data including new results and a preliminary Italian secular variation curve, *Geophys. J. Int.*, 167(3), 1160–1171, doi:10.1111/j.1365-246X.2006.03150.x.
- Thellier, E. (1938), Sur l'aimantation des terres cuites et ses applications géophysiques, Thèse de doctorat, Paris, Ann. Inst. Phys. du Globe, Paris, 16, 157–302.
- Thellier, E., and O. Thellier (1959), Sur l'intensité du champ magnétique terrestre dans le passé historique et géologique, *Ann. Geophys.*, 15, 285–376.
- Valet, J. P. (2003), Time variations in geomagnetic intensity, *Rev. Geophys.*, 41(1), 1004, doi:10.1029/2001RG000104.
- Valet, J. P., E. Herrero-Bervera, J.-L. LeMouél, and G. Plenier (2008), Secular variation of the geomagnetic dipole during the past 2000 years, *Geochem. Geophys. Geosyst.*, 9, Q01008, doi:10.1029/2007GC001728.
- Yang, S., H. Odah, and J. Shaw (2000), Variations in the geomagnetic dipole moment over the past 12 000 years, *Geophys. J. Int.*, 140(1), 158–162, doi:10.1046/j.1365-246x.2000.00011.x.
- Zanarini, I., C. M. Batt, P. Lanos, D. H. Tarling, and P. Linford (2007), Archaeomagnetic secular variation in the UK during the past 4000 years and its application to archaeomagnetic dating, *Phys. Earth Planet. Inter.*, 160(2), 97–107, doi:10.1016/j.pepi.2006.08.006.

A. Chauvin and P. Lanos, Géosciences-Rennes, UMR6118, Université de Rennes I, CNRS, Campus de Beaulieu, Bât. 15, F-35042 Rennes CEDEX, France.

M. Gómez-Paccard, Facultat de Geologia, Departament d'Estratigrafia, Paleontologia i Geociències Marines, Universitat de Barcelona, c/Martí i Franquès s/n, E-08028 Barcelona, Spain. (mgomezpaccard@ub.edu)

J. Thiriot, Laboratoire d'archéologie médiévale méditerranéenne, UMR6572, Maison méditerranéenne de Sciences de l'Homme, CNRS, F-13094, Aix-en-Provence CEDEX 2, France.